

Geometric, thermal, and temporal constraints on the tectonic evolution of Bare Mountain, Nevada

David A. Ferrill Center for Nuclear Waste Regulatory Analyses,
John A. Stamatakos 6220 Culebra Road, San Antonio, Texas 78238

Alan P. Morris Department of Earth and Physical Sciences, The University of
Texas at San Antonio, San Antonio, Texas 78249

Raymond A. Donelick Donelick Analytical, 4819 Katy-Hockley Road, Katy, Texas 77493

Ann E. Blythe Department of Geological Sciences, University of Southern
California, Los Angeles, California 90089

Sidney M. Jones Center for Nuclear Waste Regulatory Analyses,
Kathy Spivey 6220 Culebra Road, San Antonio, Texas 78238

ABSTRACT

Outcrop patterns, macro- and mesoscale fold axes, fault-bedding cutoffs, and fault branch lines throughout central and northern Bare Mountain, Nevada, consistently plunge to the northeast at 20-40°. Structural elements exhibiting this plunge include both

contractional and extensional deformation and span approximately 300 m.y. of geologic time (Permian-Tertiary). Confirmation that this northeast plunge was developed relatively late in the history of Bare Mountain comes from paleotemperature estimates using peak metamorphic mineral assemblages, calcite twin characteristics and conodont color alteration indices. Finally, cooling ages from both apatite and zircon fission track analyses indicate Eocene through Miocene crustal attenuation and exhumation consistent with the timing and style of plunge development. The regional pattern of middle to late Miocene exhumation west and northwest of Bare Mountain indicates that Bare Mountain forms the easternmost part of a large west-directed detachment system involving the Bullfrog Hills and Funeral Mountains. It is likely that early development of this detachment fault system caused the northeast tilting of Bare Mountain, which resides in the footwall of the system. In light of this interpretation, fault architecture within Bare Mountain, previously considered to be dominated by right-lateral strike slip or oblique slip faults, is reinterpreted here as a down-to-the-southeast normal fault system, subsequently tilted to the northeast to produce the present-day east dips of faults and north dips of bedding. Equivalent Paleozoic and Precambrian strata beneath the Miocene tuff section at Yucca Mountain may be cut by faults similar to those recognized in Bare Mountain. These faults are expected to dip steeply southeastward in their unrotated state (at depth beneath Yucca Mountain) and may provide blind seismic sources. We conclude that the M5.6 1992 Little Skull Mountain earthquake, at a depth of about 10 km on a fault plane that strikes 055 and dips 56° to the southeast, occurred on one such fault, and may be part of a larger buried fault population within the pre-Tertiary strata of the Yucca Mountain region.

INTRODUCTION

Bare Mountain, in southwestern Nevada approximately 15 km west of the proposed site for a permanent geological repository for high-level radioactive waste at Yucca Mountain (Fig. 1), is a block of Precambrian and Paleozoic metasedimentary rocks that provides an interesting glimpse of the pre-Tertiary basement in this part of Nevada. Bare Mountain forms the footwall of at least two extensional fault systems: (1) a northwest-directed (top-to-the-northwest) extensional fault system and (2) the Bare Mountain fault, a down to the east normal fault. The northwest- or west-northwest-directed detachment system is most likely the principal structure responsible for exhumation of Bare Mountain and is probably related to the Bullfrog Hills/Boundary Canyon/Funeral detachment system (Hamilton, 1988; Maldonado, 1990; Hoisch and Simpson 1993; Hoisch et al. 1997). The Fluorspar Canyon fault, which bounds Bare Mountain to the north, is also part of the Bullfrog Hills detachment system (Figs. 1 and 2) which was active during the Miocene (13-7.5 Ma) (Maldonado, 1990; Hoisch et al., 1997). It may have accommodated as much as 275% extension of the Tertiary volcanic sequence within the Bullfrog Hills northwest of Bare Mountain (Maldonado, 1990). The Bare Mountain fault is an east-directed (down-to-the-east) normal fault, active from the Miocene into the Holocene (Snyder and Carr, 1984; Swadley et al., 1984; Carr and Parrish, 1985; Reheis, 1986; Ferrill et al., 1996b). It has previously been interpreted as a late-stage high angle fault that cuts a low angle west-directed extensional detachment at the base of the Tertiary sequence (Scott, 1990) or, alternately, as the surface exposure of a folded regional detachment that extends eastward beneath Crater Flat and Yucca Mountain and westward over Bare Mountain and beneath the Bullfrog Hills as the Bullfrog Hills detachment (Hamilton, 1988). Considerable evidence, however, now

indicates that Bare Mountain has been exposed at least since the middle Miocene (Carr and Parrish, 1985; Simonds et al., 1995). We interpret the Bare Mountain fault as a listric normal fault that soles at depth into a low-angle fault or ductile shear zone near the brittle/ductile transition to the east (Ferrill et al., 1996a) and as such, a first-order structure that may directly controls activity of faults at Yucca Mountain. In this interpretation, faults mapped in the Miocene tuffs at Yucca Mountain accommodate hangingwall deformation related to motion along the Bare Mountain fault.

Reconstructions of the deformation history of Bare Mountain are complicated by structural complexities involving contractional faulting and folding, several generations of extensional faulting, locally small-scale and regionally large scale vertical axis rotations, and ambiguities surrounding both timing of deformation and sense of fault slip. In the present study we report on recent field and laboratory analyses of the deformation history of faulting that bear directly on interpretations of the pre-Miocene tectonic history of Bare Mountain. These results also have important implications for the neotectonic setting of Yucca Mountain. Specifically, new structural and thermometry data coupled with previously published metamorphic data demonstrate that much of the apparent complexity of faulting within Bare Mountain is due to a northeast plunge of the northern two-thirds of the mountain (north of the Panama thrust). We invoke footwall deformation during early phases of displacement to explain initial exhumation of the southwest flank of Bare Mountain and the resulting 20-40° northeastward structural plunge, possibly along a cryptic southwest-dipping extensional fault. Viewed in this context, the western side of Bare Mountain exposes an oblique cross section through a northeast-plunging normal fault system. This interpretation is supported by new apatite and zircon fission track dates, which provide new

constraints on the timing of deformation within Bare Mountain and its subsequent exhumation. These new timing constraints on early Tertiary extensional deformation within Bare Mountain coupled with recognition of the northeast plunge reveals a subregional fabric of southeast-dipping faults in the Paleozoic section that provides an analog for buried (blind) seismic sources in the Yucca Mountain region. The 1992 Little Skull Mountain earthquake is considered as a possible example of slip on one such fault.

GEOLOGIC FRAMEWORK

Bare Mountain exposes a more than 7 km thick section of Late Proterozoic through Mississippian marine sedimentary rocks (Monsen et al., 1992) (Fig. 2). The pre-Tertiary sequence is part of the continental shelf miogeocline on the western margin of the North American craton in Late Proterozoic to Mississippian time (e.g., Poole et al., 1992; Burchfiel et al., 1992) (Fig. 2). The youngest Paleozoic strata exposed at Bare Mountain are Mississippian and Late Devonian (?) rocks in northeast Bare Mountain. Older strata are exposed to the south and west. The Precambrian and Paleozoic strata have been intruded by minor Cretaceous, Oligocene (?), and Miocene intrusive rocks (Monsen et al., 1992). Eruption of a variety of pyroclastic rocks, with minor rhyolitic flows and basalts, occurred during the middle to late Miocene (> 15–7.5 Ma; e.g., Sawyer et al., 1994), initiating roughly coevally with the onset of extreme regional extension in the Basin and Range (Wernicke, 1992).

Using metamorphic mineral assemblages, Monsen (1983) showed highest metamorphic grades in the northwestern corner of Bare Mountain where the hangingwall of the subhorizontal Conejo Canyon detachment (Fig. 1) contains staurolite-bearing amphibolite facies Cambrian strata

(peak temperature >520 °C) and is juxtaposed against biotite-zone greenschist facies Cambrian and late Proterozoic strata (peak temperature 350-400 °C) in the footwall. The origin and tectonic history of the Conejo Canyon detachment is somewhat enigmatic. Structural and metamorphic relationships described and mapped by Monsen (1983), Carr and Monsen (1988), and Monsen et al. (1992) illustrate the complex geologic relationships of the Conejo Canyon detachment system. Juxtaposition of staurolite-bearing strata over garnet-bearing strata suggests contractional displacement, whereas removal of stratigraphic section suggests extensional displacement. Another major fault that juxtaposes discordant metamorphic grades is the steep east-dipping Gold Ace Mine fault (Fig. 3). Pelitic beds west of the Gold Ace Mine fault tend to have strong slaty cleavage. Shale layers in the Nopah Formation east of the Gold Ace Mine fault typically exhibit a non-penetrative planar cleavage that is clearly of lower grade. The non-metamorphosed appearance of shaly units east of the Gold Ace Mine fault suggests sub-greenschist facies peak metamorphic conditions (<300 °C) for Cambrian and Ordovician strata exposed immediately east of the Gold Ace Mine fault. The juxtaposition of biotite-zone greenschist facies and sub-greenschist facies across the Gold Ace Mine fault represents a minimum of 100 °C difference in metamorphic temperature which equates to 3.3 km of vertical displacement, assuming an average Basin and Range geothermal gradient of 30 °C/km (Sass et al., 1994). Similarly, the geologic cross section drawn across Bare Mountain indicates 3 km of vertical displacement along the Gold Ace Mine fault based on stratigraphic offset (Fig. 3).

Paleotemperature estimates from conodont color alteration index (CAI) data for Bare Mountain (Grow et al., 1994) show trends similar to those from metamorphic data. Lowest CAI values (4-4.5) in northeastern Bare Mountain (at Meiklejohn Peak) correlate to maximum

temperatures of 190-250 °C (Harris et al., 1978; Grow et al., 1994). Conodont CAI values from south and west of Meiklejohn Peak generally range between 5 and 7 suggesting peak temperatures >300 °C (Grow et al., 1994; Rehebian et al., 1987). In contrast, conodonts from samples of Paleozoic carbonates from borehole UE25P#1 (Fig. 1) at Yucca Mountain yielded CAI value of 3 (Grow et al., 1994), indicating peak temperature of 110-200 °C (after Harris et al., 1978), considerably lower than any peak temperature estimated from Bare Mountain itself. This contrast demonstrates considerably shallower maximum burial for Paleozoic rocks at Yucca Mountain.

FAULTS WITHIN BARE MOUNTAIN

Faults in and surrounding Bare Mountain represent a protracted deformation history from the late Paleozoic through the present. Pre-Tertiary deformation within Bare Mountain is represented by contractional structures that include the Meiklejohn Peak thrust, the Panama thrust, and perhaps the Conejo Canyon detachment system (Monsen, 1983; Monsen et al., 1992; Snow, 1992; Caskey and Schweickert, 1992). Displacement histories of the contractional deformation on the Meiklejohn Peak and Conejo Canyon faults are complicated by subsequent reactivation or these features as extensional faults during the Tertiary (Monsen et al., 1992).

The dominant internal structural fabric of present day Bare Mountain is defined by bedding that dips to the north and extensional faults that dip to the east (Monsen, 1983; Carr and Monsen, 1988; Monsen et al., 1992). Monsen et al. (1992) noted that "east-dipping normal faults may have [a] substantial component of right-lateral strike-slip displacement". The plunge-perpendicular cross section in Figure 3 illustrates that several of the faults within Bare Mountain extend to depths > 10 km. The largest-displacement fault of the east-dipping set is the Gold Ace

Mine fault which has approximately 3 km of displacement (Fig. 3). Many of the normal faults mapped within Bare Mountain are curved in plunge-perpendicular profile and these bends can be seen in the geologic map of Monsen et al., 1992 (Fig. 2). Most fault curvatures in Bare Mountain are downward-flattening (listric) bends, however some faults have downward steepening (antilistric) bends (Fig. 3).

The subhorizontal Conejo Canyon detachment contains a dismembered sequence of uppermost Late Proterozoic to lowermost Paleozoic rocks in its hangingwall and apparently cuts faults of the predominant east-dipping (Eocene) fault set (Monsen et al., 1992). Consistency of timing of exhumation in the middle Miocene, as constrained by apatite fission track thermochronometry, indicates that major displacement on the Conejo Canyon detachment system was prior to apatite cooling to 110 °C at about 13 Ma (see section on Apatite Fission Track Thermochronology).

GEOMETRIC RELATIONSHIPS THAT DEFINE NORTHEAST PLUNGE

Several types of structural data define a northeastward structural plunge of Bare Mountain, including outcrop and large scale fold axes, fault-bedding intersections, cleavage-bedding intersections, and synthetic and antithetic fault intersections. Bedding orientations from Bare Mountain (Monsen et al., 1992), contoured and fitted by best-fit great circles (Fig. 4), define a northeastward plunge to the axis of bedding tilt in northern and central Bare Mountain, and an eastward plunge in southern Bare Mountain. The overall bedding tilting is the composite result of both folding and fault block tilting. Bedding orientations around the large late Paleozoic contractional fold at Meiklejohn Peak (Fig. 5A) define a 33° plunge toward 039° (Fig. 5B).

Bedding cutoff lines on early Tertiary faults at virtually all scales within northern Bare Mountain have relatively consistent plunges that are similar to the plunge of the Meiklejohn Peak anticline. The intersection between the dominant north dip of bedding in central and northern Bare Mountain and east dip of extensional faults, such as the Gold Ace Mine fault, plunges northeastward (Figs. 6 and 7). At well-exposed outcrops, fault and bedding intersections clearly demonstrate the northeastward plunge (Fig. 7A). For example, fault and bedding orientations from an extensional fault system exposed in the hangingwall of the Gold Ace Mine fault define a plunge of 37° toward azimuth 042° (Fig. 7B). This plunge of fault and bedding intersections in the hangingwall of the Gold Ace Mine fault persists down to the mesoscopic scale where small faults intersect bedding to define a northeastward plunge of 36° toward 041° (Fig. 8). It seems unlikely that contractional, extensional, and strike-slip structural axes at Bare Mountain independently formed plunging northeastward over approximately 300 m.y. of geologic time. Rather, we suggest that the structural plunge developed during the Tertiary by northeastward tilting of originally near-horizontal structural axes, well after significant contractional and extensional deformation. Paleomagnetic analyses (Stamatakos et al., this issue) further support an interpretation that the plunge was produced by northeastward tilting, well after these rocks were folded and faulted during Paleozoic and Mesozoic deformations.

CALCITE DEFORMATION GEOTHERMOMETRY

Calcite deformation geothermometry shows a pattern of increasing deformation temperature from northeast to southwest that further supports our interpretation of a northeast plunge of Bare Mountain. Calcite deformation geothermometry utilizes temperature dependence

of calcite twinning and recrystallization to estimate temperatures during deformation. The roles of twin nucleation (formation of new twins), twin growth (widening of existing twins), and dynamic recrystallization during deformation are controlled by deformation temperature (Ferrill, 1991; Burkhard, 1993). As temperatures increase ($>150-200\text{ }^{\circ}\text{C}$), growth by widening of existing twins is favored over nucleation of new twins. Dynamic recrystallization of calcite initiates at even higher temperatures ($>250\text{ }^{\circ}\text{C}$). Several distinct temperature regimes for twinning and recrystallization have been identified from empirical studies (Ferrill, 1991; Burkhard, 1993). These deformation regimes, and corresponding deformation temperatures, can be identified based on microstructural assemblages (specifically twin types) present in coarse-grained limestone. Type I twins (typical of deformation temperatures $<200\text{ }^{\circ}\text{C}$) are generally straight and thin. Thin twins typically have no visible width of twinned material but, instead, appear in thin section as thin black lines. Type II twins (typical of $150-300\text{ }^{\circ}\text{C}$ deformation temperatures) are thick, commonly $\gg 1\text{ mm}$, and are straight to slightly lensoid in shape. Type III twins (typical of deformation temperatures $>200\text{ }^{\circ}\text{C}$) are thick, having different extinction in thin section, and are lensoid in shape (tapering toward grain boundaries). Commonly, type III twins are curved and may themselves be twinned, and nearly completely twinned grains are common at large strains. Type IV twins (typical of deformation temperatures $>250\text{ }^{\circ}\text{C}$) are thick and partially to completely recrystallized; calcite grains and twin boundaries are commonly interdigitated or defined by trails of small subgrains.

Samples of coarse-grained limestone for this study were collected from Cambrian through Devonian carbonates from sites distributed throughout Bare Mountain (Fig. 9). Oriented thin sections were then prepared and examined optically using a standard petrographic microscope to

characterize the dominant twin types. Deformation temperatures were inferred using the approach of Burkhard (1993) in which the first appearance of microstructures is used as the basis for estimating peak deformation temperature.

The distribution of calcite microstructures provides evidence for several distinct deformation temperature domains within Bare Mountain (Fig. 9). Type I twins (e.g., Fig. 10A), which indicate deformation temperatures <200 °C, predominate only in the northeast corner of Bare Mountain, within and near Meiklejohn Peak, both above and below the Meiklejohn Peak thrust. Type II twins (e.g., Fig. 10B), indicating deformation temperatures of 150-300 °C, were found along southeastern Bare Mountain in the hangingwall (south of) the Panama Thrust (Fig. 9). Type III twins (e.g., Fig. 10C), indicating deformation temperatures >200 °C, are common near the crest of central Bare Mountain, in the hangingwall of the Gold Ace Mine fault (location C in Fig. 9). Complete grain recrystallization and type IV twins (e.g., Fig. 10D), indicating deformation temperatures >250 °C, are found in the hangingwall of the Gold Ace Mine fault along the southwestern flank of Bare Mountain, and in the footwall of the Fluorspar Canyon detachment in the northwest corner of Bare Mountain consistent with high temperatures recorded by metamorphic mineral assemblages and conodont CAI data. These calcite microstructural data indicate lowest deformation temperatures in the northeast corner of Bare Mountain, and higher maximum deformation temperatures to the south and west.

If we assume a geothermal gradient and a surface temperature at the time of calcite twinning, constraints on the depth at the time of twinning can be calculated. For example, if we assume an average surface temperature of 10 °C and a geothermal gradient of 30 °C/km during twinning, then the depth during twinning and recrystallization for rocks presently exposed along

the western Bare Mountain (D in Fig. 9) would have been at depths >8 km. Based on the same assumptions, depth would have been >6.5 km (and probably <8 km based on lack of recrystallization in these samples) during formation of type III twins in central Bare Mountain (C in Figure 9), >5 km (and probably <6.5 km based on lack of type III twins or recrystallization in these samples) for type II twin sites along southeastern Bare Mountain, and <6.5 km for type I twin sites at and near Meiklejohn Peak in northeast Bare Mountain.

APATITE FISSION TRACK THERMOCHRONOLOGY

Thirty-one samples were collected at Bare Mountain for apatite fission track analysis using fluorine rich apatites. Samples were taken from a variety of exposed clastic and igneous rocks including the Late Proterozoic Stirling Quartzite, Late Proterozoic to Cambrian Wood Canyon Formation, Cambrian Zabriskie Quartzite, Ordovician Eureka Quartzite, Mississippian to Devonian Eleana Formation, a Cretaceous granite sill, an Oligocene diorite dike, and several Miocene silicic porphyry dikes. Sample locations were chosen to provide the maximum spatial and topographic coverage possible (Figs. 1 and 11). For comparison to the Bare Mountain results, and to test for the proposed tectonic reconstruction of the Striped Hills with Bare Mountain (Caskey and Schweickert, 1992), two samples were also collected from the Zabriskie Quartzite and Wood Canyon Formation in the Striped Hills (Fig. 1).

Reliable apatite fission track ages were obtained (methods described in Appendix 1) from 31 of the 33 samples; 29 from Bare Mountain and two from the Striped Hills (Fig. 12; Table 1). Samples BMN-21 and BMW-13 had only one or two spontaneous tracks and both yielded distinctly young fission track ages compared to the other 27 samples from Bare Mountain. We

therefore do not consider them representative and do not use them in the following discussions.

Except for the Miocene silicic porphyry dikes, all apatite ages are significantly younger than the host rocks indicating that these rocks were heated above the temperatures required for total fission track annealing in the apatites well after original deposition of the host sedimentary deposit. Thus, the ages are not inherited (e.g., from rocks of a previously eroded terrane). Rather they reflect cooling of the host rocks through apatite closure temperatures, presumably during exhumation.

The three samples from silicic porphyry dikes (BMN-16, BME-2, and BME-6) apparently preserve primary cooling of the dikes after they were intruded into Bare Mountain in the Miocene. The ages agree with conventional K/Ar and $^{40}\text{Ar}/^{39}\text{Ar}$ dates from several of these same dikes (within the bounds of analytical precision). The radiometric dates from the silicic porphyry dikes range between 13.8 to 14.9 Ma (Marvin et al., 1989; Noble et al., 1991; Monsen et al., 1992; Weiss, 1996) compared to an average 14.0 ± 1.9 (1s) Ma apatite fission track age. However, this age also overlaps with the proposed 11 to 12.5 Ma hydrothermal and epithermal alterations of these dikes at Bare Mountain (Weiss, 1996) and thus we cannot rule out the possibility that the apatite ages were marginally affected by such alterations. However, because such hot fluid-rock interactions are probably short-lived (e.g., Dorobek, 1989) and apatite annealing follows an Arrhenius temperature-time relationship with a rather steep gradient (e.g., Green et al., 1985), it is unlikely that the hydrothermal or epithermal fluid kept the dikes hot enough for a long enough period of time to completely anneal apatite fission tracks.

Apatite fission tracks from the other 26 samples at Bare Mountain yielded Miocene ages ranging between 7.9 and 17.1 Ma (Table 1 and Fig. 11), although 80% of the ages fall between

10 and 15 Ma. The distribution of ages appears to be normal (Fig. 12a) with a weighted mean age of 12.3 ± 0.4 (1s) Ma and an arithmetic mean age of 12.9 ± 2.4 (1s) Ma. We note little spatial variability in the fission track ages and track lengths. The track lengths and ages do not vary as a function of elevation, although a pronounced elevation effect is not necessarily expected in this case because of the limited relief (~ 1000 m). Thus, fission track ages for Bare Mountain can be interpreted without regard to sample elevation. In addition, apatite fission track ages appear to be independent of the sample's geographical position across Bare Mountain. Given the sample density (29 samples over approximately 100 km^2) and lack of any spatial or elevation control to the ages, we infer that the variability in these ages is representative of the overall variability inherent in the population of apatite ages at Bare Mountain. In other words, apatite fission track ages probably cannot be known to better than about ± 2.4 Ma. There are no significant offsets of apatite ages across either the Gold Ace Mine or Conejo Canyon faults. Thus, significant fault displacements recorded by the metamorphic and conodont temperature data appear to have occurred prior to the middle Miocene at temperatures in excess of those required to totally anneal fission tracks in the apatite grains.

Natural confined track lengths in the Bare Mountain samples ranged between 9.4 and 14.8 mm (Table 1). The distribution of track lengths is also normal (Fig. 12b) with a mean of 13.3 ± 1.0 mm. These relatively long mean track lengths suggest rapid cooling of the samples as they passed through the apatite closure temperature (e.g. Crowley et al., 1989). There is a suggestion in the data that track lengths are slightly longer in the northern half and especially in the northwest corner of the Mountain, so cooling may have been even more rapid there. Such rapid cooling suggests tectonic as opposed to erosional exhumation of Bare Mountain.

In contrast to Bare Mountain, the two fission track ages and their corresponding track lengths from the Striped Hills indicate a decidedly different thermal history (Fig. 12c). Both samples yield Cretaceous ages and both samples have significantly shorter track lengths (Table 1). The different thermal histories at Bare Mountain and the Striped Hills cast doubt on a simple reconstruction juxtaposing the Striped Hills with Bare Mountain, assuming that the two ranges were once adjacent segments of a pre- Basin and Range (Sevier age) fold and thrust belt (e.g., Caskey and Schweickert, 1992).

ZIRCON FISSION TRACK THERMOCHRONOLOGY

Samples for zircon fission track analysis were collected at 11 sites distributed across Bare Mountain (Figs. 1 and 13) from a variety of exposed clastic rocks including the Wood Canyon, Stirling and Zabriskie formations as well as one site from a Miocene silicic porphyry dike. Because we were especially interested in constraining the age of motion along the Meiklejohn Peak thrust and the Gold Ace Mine fault, sample locations were chosen to provide coverage of those structures. Each zircon sample site corresponds directly with an apatite sampling site.

The annealing characteristics of zircon fission tracks are not as well constrained as for apatite fission tracks. A recent field study suggests that the zircon fission-track partial annealing zone ranges from 230 °C to 330 °C (Tagami and Shimada, 1996). Foster et al. (1993) obtained estimates of the zircon fission-track closure temperature of approximately 240 °C to 260 °C by comparing K-feldspar $^{40}\text{Ar}/^{39}\text{Ar}$ analyses with zircon fission-track analyses of several Basin and Range samples. In this study, we consider the zircon fission track data in terms of zircon partial annealing zone of 230 °C to 330 °C and a closure temperature of approximately 250 °C.

Zircon fission track ages from Bare Mountain (methods described in Appendix 2) can be divided into five groups (Figs. 13 and 14); Pennsylvanian-Permian (275-300 Ma) ages from the northeast corner, Eocene (40-45 Ma) ages from the southern part of the range, Oligocene (25-35 Ma) ages from north-central part of the range, Miocene (14-16 Ma) cooling ages from clastic rocks in northwest Bare Mountain, and a Miocene (12 Ma) dike cooling age from northeast Bare Mountain.

Similar to the apatite ages, nearly all the zircon fission track ages are much younger than the ages of their host rocks, suggesting that the host rocks were heated above the total fission track annealing temperatures of zircon well after deposition. Thus, like the apatites ages, the zircon fission track ages are not inherited from a previously eroded terrane, but instead reflect cooling of the host rocks, presumably during exhumation. The lone exception is the sample from the silicic porphyry dike (BME-2) which yields a zircon fission track age of 11.9 ± 1.2 Ma (1s) compared to the apatite fission track age of 12.3 ± 3.2 Ma (1s). As discussed above, we cannot determine absolutely whether this age reflects primary cooling (after intrusion) or secondary cooling (after hydrothermal and epithermal alteration).

AGE AND SEQUENCE OF FAULTING AND NORTHEAST TILTING

The age and sequence of faulting and tilting of Bare Mountain is constrained by a wide variety of data discussed above and summarized in Figure 15. Northeast tilting of Bare Mountain occurred after development of thermally controlled microstructural zonation of deformed calcite, contractional folding, and subsequent acquisition of a secondary magnetization of the Meiklejohn Peak fold (Stamatakis et al., this issue), as well as early extensional faulting (e.g., Gold Ace

Mine fault and related faults). In contrast, northeast tilting predated cooling of Bare Mountain through the fluorine-rich apatite annealing temperature ($\sim 110^{\circ}\text{C}$), emplacement of vertical silicic porphyry dikes (at about 12 Ma), and acquisition of a hematite (H component) secondary magnetization (Stamatikos et al., this issue).

Pre-middle Miocene tilting of Bare Mountain preferentially exhumed progressively deeper, older, and hotter strata from northeast to southwest. Northeast tilting during or prior to the middle Miocene can be explained as footwall uplift at the breakaway beneath a detachment normal fault (e.g., Wernicke and Axen, 1988; Wernicke, 1992). The southwest flank of Bare Mountain in this interpretation was rotated (up to the southwest, down to the northeast) about a northwest-southeast horizontal axis and represents the deeply eroded footwall (breakaway) for the west-northwest-directed Bullfrog Hills/Boundary Canyon/Funeral detachment system (Hamilton, 1988; Hoisch and Simpson, 1993; Hoisch et al., 1997). Our interpretation differs from Hamilton's (1988) in that the breakaway for detachment is interpreted to be at Bare Mountain, rather than east of Bare Mountain. Therefore, Yucca Mountain was not involved in the Bullfrog Hills/Boundary Canyon/Funeral detachment systems. In Wernicke and Axen's (1988) model, footwall tilting of the breakaway occurs relatively early in response to isostatic footwall uplift associated with exhumation by the detachment. Footwall exhumation is progressively younger from the breakaway towards the hangingwall. Apatite fission track data from the lower plate of the Bullfrog Hills/Boundary Canyon/Funeral detachment system exhibit a general westward younging of cooling ages that indicate cooling and exhumation at 13 Ma from Bare Mountain (this study), 10 Ma from the Bullfrog Hills (Hoisch et al., 1997), and 6 Ma from the Funeral Mountains (Holm and Dokka, 1991; Hoisch et al., 1997). The relative spatial uniformity of

apatite fission track ages and lack of tilting of Miocene dikes in Bare Mountain suggests rather uniform Miocene exhumation without major middle Miocene or younger tilting of the range.

This leaves Eocene to Oligocene zircon fission track cooling ages (Figs. 13 and 14) unexplained by any well-documented faulting episode. These ages can be interpreted by either crustal thinning, due to displacement on the Gold Ace Mine fault and related faults, or by exhumation beneath a cryptic, southwest dipping "Amargosa Valley" fault. The Oligocene (25-35 Ma) zircon fission track cooling ages from north-central Bare Mountain (Fig. 13), in the footwall (west) of the Gold Ace Mine fault, may reflect Oligocene cooling during exhumation caused by accumulation of the 3 km of normal dip-slip displacement on the fault. Similarly, Eocene (40-45 Ma) zircon fission track cooling ages from southern Bare Mountain (Fig. 13) may represent cooling due to crustal thinning by normal faulting within the crustal section now exposed in Bare Mountain. Alternatively, the Eocene and Oligocene zircon fission track ages may reflect early exhumation of the southwest flank of Bare Mountain at the onset of tilting, in which case the Gold Ace Mine fault and related faults may have formed during Eocene exhumation described by Axen et al. (1993). These timing constraints bracket tilting of Bare Mountain between middle Eocene (or early Oligocene) and middle Miocene.

TECTONIC IMPLICATIONS

Structural style

The role of listric faulting in the Bare Mountain and Yucca Mountain area has been the source of considerable debate (e.g., Simonds et al., 1995) because of its potential for shallow seismic sources represented by shallow fault systems and the possibility that shallow fault systems

mask deeper, blind seismic sources. Cross sections by Young et al. (1993) and Ferrill et al. (1996a), based on geometric constraints, indicate the possibility of listric faults in the middle and lower parts of the brittle crust (within the pre-Tertiary section) beneath Yucca Mountain. Recent mechanical modeling indicated that such listric faults could be active in the present regional stress field (Ofoegbu and Ferrill, 1995, and in press). However, the potential for seismicity is considerably smaller on low angle fault segments than on steep segments, due to reduced rupture propagation rate on low angle fault segments (Ofoegbu and Ferrill, 1995, in press). The present study documents that listric fault systems that flatten from steep to shallow depths within the Paleozoic and Precambrian stratigraphic section are prevalent within Bare Mountain. As discussed by Elliott (1983), balanced structural models must be both admissible (constructed using the structural style observable in the region) and viable (restorable to an unstrained state). Inasmuch as Bare Mountain represents the most complete exposure of the pre-Tertiary section in close proximity to Yucca Mountain, the structural style observed in Bare Mountain represents a primary control for the admissibility of structural models that describe the pre-Tertiary rocks buried in the surrounding areas. Consider for example the scale invariance of faults at the Gold Ace Mine exposure (Figs. 7 and 8) and those in the entire northwest corner of Bare Mountain (Fig. 6). These natural examples of the structural pattern within the pre-tertiary stratigraphic section suggest that this structural style is repeated in the Paleozoic rocks covered by the Quaternary basin fill and volcanic strata at and near Yucca Mountain.

Analog for faults beneath Yucca Mountain

Timing constraints on the formation of early extensional faults in Bare Mountain indicate that faulting within western Bare Mountain occurred considerably earlier than Miocene tuff deposition, formation of the Bare Mountain fault, and faulting at Yucca Mountain and Crater Flat. Bare Mountain is within a pre-middle Miocene extensional province defined by Axen et al. (1993) which extends from the Grapevine Mountains (25 km west of Bare Mountain) to 100 km east of Bare Mountain. The implication of the relatively early normal faulting is that similar faults probably exist east of Bare Mountain, for example beneath Crater Flat, Yucca Mountain, and Jackass Flat. We interpret the northeast tilting of Bare Mountain as a local product of footwall tilting due to regional detachment faulting that has not extended eastward as far as Yucca Mountain. Therefore, in order to understand the sub-Tertiary structural fabric at Yucca Mountain, the fault orientations at Bare Mountain must be restored to their pre-tilt orientation. Restoring faults exposed near Gold Ace Mine fault (shown in Fig. 7) to their pre-tilt orientation indicates that the faults originally dipped to the southeast. These tilt-corrected orientations cluster near the maximum slip tendency in the contemporary stress field (Fig. 16; Morris et al., 1996). A possible example of slip on one such fault is the 1992 Little Skull Mountain earthquake.

The focus of the M5.6 1992 Little Skull Mountain earthquake was at a depth of about 10 km (Fig. 16; Harmsen, 1994). Nodal planes from the Little Skull Mountain earthquake and aftershocks indicate that the slip occurred on faults clustered around the slip tendency maximum in the contemporary stress field (Fig. 16). The Little Skull Mountain mainshock occurred on a southeast-dipping fault (Harmsen 1994) analogous to the faults of the east-dipping set seen in Bare Mountain. Based on scaling relationships between earthquake magnitude and fault rupture

area of Wells and Coppersmith (1994), a magnitude 5.6 earthquake represents a rupture area of approximately 36 km². A 36 km² circular rupture of this area would have a diameter of 6.8 km. The cross section in Figure 3 illustrates that several of the faults within Bare Mountain extend in the dip direction for more than 7 km and suggests that faults of this and larger dimensions are probably prevalent beneath the Miocene tuff cover between Bare Mountain and Little Skull Mountain beneath Crater Flat, Yucca Mountain, and Jackass Flats (Fig. 1).

CONCLUSIONS

New geometric, thermal, and temporal data lead to four principal conclusions regarding tectonic history and neotectonic setting of Bare Mountain and the Yucca Mountain region, in southwest Nevada.

1. Precambrian and Paleozoic strata exposed in Bare Mountain have experienced a protracted tectonic history including late Paleozoic contractional deformation, and middle Eocene to present extensional deformation.
2. Structures within Bare Mountain were tilted approximately 30-40° toward the northeast, after middle Eocene (to early Oligocene?) extension but prior to intrusion of dikes at about 14 Ma. This tilting rotated southeast-dipping normal faults to their present eastward dips. Tilting produced the NE structural plunge and lateral metamorphic- and deformation-temperature variations within the mountain. The apparent right-lateral strike-slip and oblique-slip displacements on east-dipping faults in Bare Mountain actually developed as normal dip-slip displacements on southeast-dipping normal faults accommodating northwest-southeast extension prior to northeast tilting.

3. Tilting probably represents deformation in the footwall of a southwest-dipping extensional breakaway that exhumed the southwestern flank of Bare Mountain and produced the northeast tilt by footwall uplift. We interpret this breakaway and exhumation of the southwest flank of Bare Mountain as footwall deformation beneath the regionally recognized northwest- or west-northwest-directed Bullfrog Hills/Boundary Canyon/Funeral detachment system.

4. Bare Mountain provides the best exposed examples of deformation within the pre-Tertiary sequence in the immediate vicinity of Yucca Mountain. The southwestern flank of Bare Mountain exposes a cross section approximately normal to structural plunge within the mountain and illustrates that normal faults within the mountain merge and flatten with depth to form listric fans at a range of scales. The structural history of Bare Mountain likely represents a common structural style for the pre-Tertiary section and southeastward-dipping normal faults are expected to be prevalent within the pre-Tertiary section beneath the volcanic cover in the Yucca Mountain area. The 1992 M5.6 Little Skull Mountain earthquake and associated aftershocks may represent seismic slip on faults in the pre-Tertiary sequence in orientations independently indicated based on structural data from Bare Mountain.

ACKNOWLEDGMENTS

This paper was prepared as a result of work performed at the Center for Nuclear Waste Regulatory Analyses (CNWRA) for the U.S. Nuclear Regulatory Commission (NRC) under contract number NRC-02-93-005. The activities reported here were initiated on behalf of the NRC Office of Nuclear Regulatory Research, as part of the Tectonic Processes of the Central Basin and Range research project, and continued on behalf of the Office of Nuclear Material

Safety and Safeguards. This paper is an independent product of the CNWRA and does not necessarily reflect the views or regulatory position of the NRC. We wish to thank Steve Young, Larry McKague, and Annette Mandujano for their comments and suggestions, and assistance in manuscript preparation. Technical reviews by Bob Scott, Warren Hamilton, Gerry Stirewalt, and Wes Patrick considerably improved the manuscript. We thank Anita Harris (U.S. Geological Survey) for supplying conodont data from Bare Mountain.

Appendix 1. Apatite Fission Track Analytical Methods

Each sample was reduced to sand-sized particles using a jaw-crusher and pulverizer, sieved through a 300 μm mesh, washed in water to remove clay-sized particles, and dried at 90 $^{\circ}\text{C}$ for 1 hour. After drying, any apatite present in each sample was isolated using standard gravimetric and magnetic mineral separation techniques. A minimum of two apatite grain mounts were prepared for each sample. Each grain mount consisted of some quantity of apatite grains immersed in epoxy resin that was cured at 90 $^{\circ}\text{C}$ for 1 hour. Once cured, each grain mount was polished to a glass-like finish to expose internal surfaces of the apatite grains within it. After polishing, one grain mount was immersed in 5.5N HNO_3 for 20.0 seconds (± 0.5 seconds) at 21 $^{\circ}\text{C}$ (± 1 $^{\circ}\text{C}$) to reveal each natural fission track that intersects its respective polished apatite grain surface.

Fission track ages of individual apatite grains were measured using the external detector method of analysis. Samples were irradiated simultaneously for 1 hour in position A-8 of the Texas A&M University nuclear reactor while the reactor was operating at 1 MW power output; this irradiation yielded a thermal-neutron fluence of approximately 10^{16} neutrons/ cm^2 . The mica detectors were etched in 48% HF at 24 $^{\circ}\text{C}$ (± 1 $^{\circ}\text{C}$) for 12 minutes (± 15 seconds) to reveal any induced fission tracks resulting from the induced fission of ^{235}U in the adjacent apatite grains and the CN-1 dosimeter glass, respectively.

The total etchable length of a natural fission track is a strong indicator of the integrated thermal history that the track has experienced. Fission tracks form continuously through time at a rate determined solely by the concentration of ^{238}U in the host apatite grain. As such, the distribution of total etchable fission track lengths in an apatite contains abundant information

about the time-temperature path experienced by the apatite, particularly the cooling history since the time of peak temperature. The second of two polished apatite grain mounts (rarely more) was irradiated with approximately 10^7 tracks/cm² fission fragments from a 50 μ Ci (50 microcurrie) (activity as of July, 1996) ²⁵²Cf source in a vacuum chamber to enhance the measurability of natural fission track length distributions. Only natural, horizontal, confined fission tracks in apatite with well etched ends were considered candidates for length measurement. Fission tracks for both age and length measurement were viewed in unpolarized light at 1562.5x magnification (100x dry objective, 1.25x projection tube, 12.5x oculars).

The fission track ages reported in this paper have been remeasured using grain mounts reported on earlier (Spivey et al., 1995). There were several reasons for remeasurement. First, many of the apatite grains at Bare Mountain have relatively low uranium concentrations making it difficult to measure the density of induced fission tracks on their respective mica detectors. We believe this problem introduced significant analyst-related noise in the original results. To overcome this problem in our re-analysis of the apatites, images of all apatite grains were recorded on videotape. The videotapes were then reviewed in detail (for every apatite grain dated) while tracks were simultaneously counted on the mica detector. This procedure ensured proper counting of the mica detector. Second, the original measurements were made using a series of six neutron irradiations in the laboratory carried out over two years. Although this is not believed to have introduced a great deal of noise in the data, in the re-analysis we re-irradiated all of the original grain mounts during a single neutron irradiation session. All re-analysis counting was also performed within a several-week period. Third, the zeta calibration

26/58

factor used to calculate the fission track ages for the re-analyses was determined using only age calibration standards irradiated simultaneously with the samples in this study.

Appendix 2. Zircon Fission Track Analytical Technique

Zircon grains were mounted in FEP teflon, ground to expose an interior surface of individual grains, and then polished. The grain mounts were etched in an eutectic mixture of KOH-NaOH at 220 °C for 18-24 hours. As with the apatite mounts, low-uranium muscovite sheets were used as external detectors. The 11 zircon grain mounts were sandwiched between chips of SRM-962a (the dosimetry glass) and were irradiated in the Cornell University Triga Reactor. Following irradiation, the mica detectors were etched in 48% HF for 30 minutes at 18 °C. Natural and induced tracks were measured optically (1250x magnification) with a Nikon Optiphot II microscope and a mechanized Kinitex Stage.

REFERENCES CITED

- Axen, G.J., Taylor, W.J., and Bartley, J.M., 1993, Space-time patterns and tectonic controls of Tertiary extension and magmatism in the Great Basin of the western United States: Geological Society of America Bulletin, v. 105, p. 56–76.
- Burchfiel, B.C., Cowan, D.S., and Davis, G.A., 1992, Tectonic overview of the Cordilleran orogen in the western United States, *in* Burchfiel, B.C., Lipman, P.W., and Zoback, M.L., eds., The Cordilleran orogen: Conterminous U.S.: Boulder, Colorado, Geological Society of America, Geology of North America, v. G-3, p. 407–479.
- Burkhard, M., 1993, Calcite twins, their geometry, appearance and significance as stress-strain markers and indicators of tectonic regime: A review: Journal of Structural Geology, v. 15, p. 351–368.
- Carr, M.D., and Monsen, S.A., 1988, A field trip guide to the geology of Bare Mountain, *in* Weide, D.L., and Faber, M.L., eds., This extended land: Geological Society of America Cordilleran Section Meeting, Field Trip Guidebook: University of Nevada at Las Vegas Geoscience Department Special Publication 2, p. 50–57.
- Carr, W.J., and Parrish, L.D., 1985, Geology of Drill Hole USW-VH-2, and Structure of Crater Flat, Southwestern, Nevada: U.S. Geological Survey Open-File Report 85-475.
- Caskey, S.J., and Schweickert, R.A., 1992, Mesozoic deformation in the Nevada Test Site and vicinity: Implications for the structural framework of the Cordilleran fold and thrust belt and Tertiary extension north of Las Vegas Valley: Tectonics, v. 11, p. 1314–1331.

- Crowley, K.O., Naeser, C.W., and Naeser, N.O., 1989. Fission Track Analysis: Theory and Applications. Short Course Manual, Geological Society of America Annual Meeting, St. Louis, Missouri, Geological Society of America, 269 p.
- Dorobeck, S., 1989, Migration of orogenic fluids through the Siluro-Devonian Helderberg Group during the late Paleozoic deformation: Constraints on fluid sources and implications for thermal histories of sedimentary basins: *Tectonophysics*, v. 159, p. 25-45.
- Elliott, D., 1983, The construction of balanced cross sections: *Journal of Structural Geology*, v. 5, p. 101.
- Ferrill, D.A., 1991, Calcite twin widths and intensities as metamorphic indicators in natural low temperature deformation of limestone: *Journal of Structural Geology*, v. 13, p. 667-675.
- Ferrill, D.A., Stirewalt, G.L., Henderson, D.B., Stamatakos, J.A., Morris, A.P. Wernicke, B.P., and Spivey, K.H., 1996a, Faulting in the Yucca Mountain Region: Critical Review and Analyses of Tectonic Data from the Central Basin and Range, CNWRA 95-017, NUREG/CR-6401: U.S. Nuclear Regulatory Commission, Washington, D.C.
- Ferrill, D.A., Stamatakos, J.A., Jones, S.M., Rahe, B., McKague, H.L., Martin, R.H., and Morris, A.P., 1996b, Quaternary slip history of the Bare Mountain fault (Nevada) from the morphology and distribution of alluvial fan deposits: *Geology*, v. 24, p. 559-562.
- Ferrill, D.A., Stamatakos, J.A., and McKague, H.L., 1997, Quaternary slip history of the Bare Mountain fault (Nevada) from the morphology and distribution of alluvial fan deposits: Reply: *Geology*, v. 25, p. 190.
- Fisher, R.A., 1953, Dispersion on a sphere. *Proceedings of the Royal Astronomical Society of London* A217, p. 295-305.

- Foster, D.A., Gleadow, A.J., Reynolds, S.J. and Fitzgerald, P.G., 1993, Denudation of metamorphic core complexes and the reconstruction of the transition zone, west central Arizona: Constraints from apatite fission track thermochronology: *Journal of Geophysical Research*, v. 98(B2), p. 2167-2185.
- Green, P.F., Duddy, I.R., Gleadow, A.J.W. and Tingate, P.R., 1985, Fission track annealing in apatite: Track length measurements and the form of the Arrhenius plot: *Nuclear Tracks and Radiation Measurements*, v.10, p. 323-328.
- Grow, J.A., Barker, C.E., and Harris, A.G., 1994, Oil and gas exploration near Yucca Mountain, southern Nevada, *in International High-Level Radioactive Waste Management Conference Proceedings*, American Nuclear Society, La Grange Park, Illinois, p. 1298–1315.
- Hamilton, W.B., 1988, Detachment faulting in the Death Valley region, California and Nevada, *in Carr, M.D., and Yount, J.C. eds., Geologic and Hydrologic Investigations of a Potential Nuclear Waste Disposal Site at Yucca Mountain, Southern Nevada: U.S. Geological Survey Bulletin 1790*, p. 51–85.
- Harmsen, S.C., 1994, The Little Skull Mountain, Nevada, earthquake of 29 June 1992: Aftershock focal mechanisms and tectonic stress field implications: *Bulletin of the Seismological Society of America*, v. 84, p. 1484–1505.
- Harris, A.G., Harris, L.D., and Epstein, J.B., 1978, Oil and gas data from Paleozoic rocks in the Appalachian Basin: Maps for assessing hydrocarbon potential and thermal maturity (conodont color alteration isograds and overburden isopachs): *U.S. Geological Survey Miscellaneous Investigations Series Map I-917E*, scale 1:2,500,000.

- Hoisch, T.D., Heizler, M.T., and Zartman, R.E., 1997, Timing of detachment faulting in the Bullfrog Hills and Bare Mountain area, southwest Nevada: Inferences from $^{40}\text{Ar}/^{39}\text{Ar}$, K-Ar, U-Pb and fission-track thermochronology. *Journal of Geophysical Research* (in press).
- Hoisch, T.D., and Simpson, C., 1993, Rise and tilt of metamorphic rocks in the lower plate of a detachment in the Funeral Mountains, Death Valley, California. *Journal of Geophysical Research*, v. 98, p. 6805-6827.
- Holm, D.K., and Dokka, R.K., 1991, Major late Miocene cooling of the middle crust associated with extensional orogenesis in the Funeral Mountains, California. *Geophysical Research Letters*, v. 18, p. 1775-1778.
- Horford, A.J., and Green, P.F., 1983. The Zeta Calibration of Fission Track Dating. *Isotope Geosciences*, v. 1, p. 285-317.
- Maldonado, F., 1990, Structural geology of the upper plate of the Bullfrog Hills detachment fault system, southern Nevada: *Geological Society of America Bulletin*, v. 102, p. 992-1006.
- Marvin, R.F., Mehnert, H.H., and Naeser, C.W., 1989, U.S. Geological Survey radiometric ages compilation "C", Part 3: California and Nevada: *Isochron/West*, no. 52, p. 3-11.
- Monsen, S.A., 1983, Structural evolution and metamorphic petrology of the Precambrian-Cambrian strata, northwest Bare Mountain, Nevada: Davis, California, University of California at Davis, Masters Thesis, 66 p.
- Monsen, S.A., Carr, M.D., Reheis, M.C., Orkild, P.A., 1992, Geologic Map of Bare Mountain, Nye County, Nevada: U.S. Geological Survey Miscellaneous Investigations Series, Map I-2201, scale 1:24 000.

- Morris, A.P., Ferrill, D.A., and Henderson, D.B., 1996, Slip tendency analysis and fault reactivation. *Geology*, v. 24, 275–278.
- Noble, D.C., Weiss, S.I., and McKee, E.H., 1991, Magmatic and hydrothermal activity, caldera geology, and regional extension in the western part of the southwestern Nevada volcanic field, *in* Raines, G.L., Lisle, R.E., Shafer, R.W, and Wilkerson, W.W., eds, *Geology and Ore Deposits of the Great Basin: Geological Society of Nevada, Reno, Nevada*, p. 913–934.
- Ofoegbu, G.I., and Ferrill, D.A., 1995, Mechanical analyses of a Yucca Mountain fault model, *in* Proceedings, Topical Meeting on Methods of Seismic Hazards Evaluation, Focus '95, Las Vegas, Nevada, American Nuclear Society, p. 115–124.
- Ofoegbu, G.I., and Ferrill, D.A., Mechanical analyses of listric normal faulting with emphasis on seismicity assessment. *Tectonophysics* (in press).
- Poole, F.G., Stewart, J.H., Palmer, A.R., Sandberg, C.A., Madrid, R.J., Ross, R.J., Jr., Hintze, L.F., Miller, M.M., and Wrucke, C.T., 1992, Latest Precambrian to latest Devonian time; Development of a continental margin, *in* Burchfiel, B.C., Lipman, P.W., and Zoback, M.L., eds., *The Cordilleran orogen: Conterminous United States: Boulder, Colorado, Geological Society of America, Geology of North America*, v. G-3, p. 407–479.
- Ramsay, J.G., 1967, *Folding and fracturing of rocks*: London, McGraw-Hill.
- Rehebian, V.A., Harris, A.G., and Huebner, J.S., 1987, Conodont color and textural alteration: An index to regional metamorphism, contact metamorphism, and hydrothermal alteration: *Geological Society of America Bulletin*, v. 99, p. 471–479.

- Reheis, M.C., 1986, Preliminary study of Quaternary faulting on the east side of Bare Mountain, Nye County, Nevada, *in* Geologic and Hydrologic Investigations of Yucca Mountain, Nevada: U.S. Geological Survey Open-File Report 86-576, p. 103–111.
- Sass, J.H., Lachenbruch, A.H., Galanis, S.P., Jr., Morgan, P., Priest, S.S., Moses, T.H., Jr., and Munroe, R.J., 1994, Thermal regime of the southern Basin and Range Province: Heat flow data from Arizona and the Mojave Desert of California and Nevada: *Journal of Geophysical Research*, v. 99 (B11), p. 22,093–22,229.
- Sawyer, D., Fleck, R.J., Lanphere, M.A., Warren, R.G., Broxton, D.E., and Hudson, M., 1994, Episodic caldera volcanism in the Miocene southwestern Nevada volcanic field: Revised stratigraphic framework, $^{40}\text{Ar}/^{39}\text{Ar}$ geochronology and implications for magmatism and extension: *Geological Society of America Bulletin*, v. 106, 1304–1318.
- Scott, R.B., 1990, Tectonic setting of Yucca Mountain, southwest Nevada, *in* Wernicke, B.P., ed., Basin and Range extensional tectonics near the latitude of Las Vegas, Nevada: Boulder, Colorado, Geological Society of America Memoir 176, p. 251–282.
- Simonds, F.W., Fridrich, C.J., Hoisch, T.D., and Hamilton, W.B., 1995, A synthesis of detachment fault studies in the Yucca Mountain Region, *in* Proceedings, Topical Meeting on Methods of Seismic Hazards Evaluation, Focus '95, Las Vegas, Nevada, American Nuclear Society, p. 107–114.
- Snow, J.K., 1992, Large-magnitude Permian shortening and continental-margin tectonics in the southern Cordillera: *Geological Society of America Bulletin*, v. 104, p. 80–105.
- Snyder, D.B. and Carr, W.J., 1984, Interpretation of gravity data in a complex volcano-tectonic setting, south-western Nevada: *Journal of Geophysical Research*, v. 89, p. 10,193–10,206.

Spivey, K.H., Ferrill, D.A., Stamatakos, J., Morris, A.P., Donelick, R.A., and Young, S.R., 1995, Uplift and cooling history of Bare Mountain, Nevada, from apatite fission track thermochronology. Geological Society of America Abstracts with Programs, v. 27, no 6, p. A-389.

Stamatakos, J.A., Ferrill, D.A., and Spivey, K.H. (in review). Paleomagnetic constraints on the tectonic history of Bare Mountain, Nevada. Geological Society of America Bulletin.

Swadley, W.C., Hoover, D.L., Rosholt, J.N., 1984, Preliminary report on late Cenozoic faulting and stratigraphy in the vicinity of Yucca Mountain, Nye County, Nevada: U.S. Geological Survey Open-file Report 84-788, 42 p.

Tagami, T., and Shimada, C., 1996, Natural long-term annealing of the zircon fission track system around a granitic pluton: Journal Geophysical Research, v. 101, p. 8245-8255.

Weiss, S. I., 1996, Hydrothermal activity, epithermal mineralization and regional extension in the southwestern Nevada volcanic field [Ph.D. dissertation], Reno, Nevada, University of Nevada at Reno, 212 p.

Wells, D.L., and Coppersmith, K.J., 1994, New empirical relationships among magnitude, rupture length, rupture width, rupture area, and surface displacement: Seismological Society of America Bulletin, v. 84, p. 974-1002.

Wernicke, B., and Axen, G.J., 1988, On the role of isostasy in the evolution of normal fault systems. Geology, v. 16, p. 848-851.

- Wernicke, B., 1992, Cenozoic extensional tectonics of the U.S. Cordillera, *in* Burchfiel, B.C., Lipman, P.W., and Zoback, M.L., eds., *The geology of North America, Volume G3: The Cordilleran orogen; Conterminous United States*: Boulder, Colorado, Geological Society of America, p. 553–581.
- Woodcock, N.H., 1977, Specification of fabric shape using an eigenvalue method: *Geological Society of America Bulletin*, v. 88, 1231–1236.
- Young, S.R., Morris, A.P., Stirewalt, G., 1993, Geometric analysis of alternative models of faulting at Yucca Mountain, Nevada: *in* *International High-Level Radioactive Waste Management Conference Proceedings*, American Nuclear Society, La Grange Park, Illinois, p. 1818–1825.

FIGURE AND TABLE CAPTIONS

Figure 1. Simplified geologic map showing relationship of Bare Mountain with respect to Crater Flat, Yucca Mountain, and Little Skull Mountain. Dashed line labeled LSM indicates surface projection of blind rupture plane of the 1992 M5.6 Little Skull Mountain earthquake (Harmsen, 1994). Star shows epicenter of Little Skull Mountain earthquake (after Harmsen, 1994).

Figure 2. Geological map of Bare Mountain (after Monsen et al., 1992) showing the line of section A-A'.

Figure 3. Plunge-perpendicular cross section of Bare Mountain along section line A-A' (see Fig. 2 for location). Stratigraphic contacts and faults mapped by Monsen et al (1992) were projected parallel to structural plunge, from southwest of cross-section line A-A' onto a plunge perpendicular plane along A-A'.

Figure 4. Structural domain map of Bare Mountain based on data in Monsen et al. (1992). Domain boundaries are drawn primarily on the basis of major faults. Lower hemisphere, equal-area stereographic projections are plotted for poles to bedding for each domain. Squares represent the poles to the best-fit great-circles (minimum eigenvector of the distribution) and represent the averaged fold axis for each domain (Fisher, 1953; Ramsay, 1967; Woodcock, 1977).

Figure 5. (A) Photograph taken looking northeast at profile through Meiklejohn Peak fold, northeastern Bare Mountain. See Fig. 2 for location. (B) Interpreted photograph of the Meiklejohn Peak fold. Inset lower hemisphere, equal-area stereographic projection illustrates poles to bedding (squares). The northeastward plunge of Meiklejohn Peak fold axis (dot) is defined by pole to best-fit great circle for poles to bedding.

Figure 6. Geologic map of northwest Bare Mountain illustrating relationships between the Conejo Canyon detachment, the Gold Ace Mine fault, and other normal faults parallel to the Gold Ace Mine fault.

Figure 7. (A) Map of extensional imbricate fault system in the hangingwall of the Gold Ace Mine fault. See Fig. 6 for location. (B) Lower hemisphere equal area stereographic projection illustrates poles to normal faults (triangles) and poles to antithetically dipping bedding (squares). The best-fit great circle fits poles to faults and bedding and defines the northeast plunge of the intersection of faults and bedding (dot) at this exposure.

Figure 8. Field sketch and lower hemisphere equal area stereographic projection of bedding and mesoscopic extensional faults exposed in oblique cross section. See Fig. 6 for location. Inset stereonet illustrates poles to normal faults (triangles) and poles to antithetically dipping bedding (squares) on an equal area, lower hemisphere projection. The best-fit great circle fits poles to faults and bedding and defines the northeastward plunge of the intersection of faults and bedding (dot) at this exposure.

Figure 9. Map of calcite-twin geothermometry sample sites. Calcite microstructures indicate lowest deformation temperature in the northeast corner of Bare Mountain and laterally increasing deformation temperatures toward the south and west across the mountain. A, B, C, and D indicate sample locations for photomicrographs shown in Fig. 10.

Figure 10. Photomicrographs of microstructures in calcite (sample locations given in Fig. 9). Dominance of crystal-plastic deformation by thin twins illustrated in (A) and (B) indicates low temperature deformation at temperatures <200 °C. (C) Thick twins and the presence of dynamically recrystallized calcite indicate deformation temperature >250 °C. (D) Complete recrystallization of calcite indicates deformation temperature $\gg 250$ °C.

Figure 11. Map of Bare Mountain, Nevada, with apatite fission track ages shown. Results from samples BMW-13 and BMN-21 were considered unreliable and not used further (see text for discussion).

Fig. 12. Plots of apatite fission track data from Bare Mountain and Striped Hills, Nevada.

Fig. 13. Map of Bare Mountain, Nevada, with zircon fission track data shown.

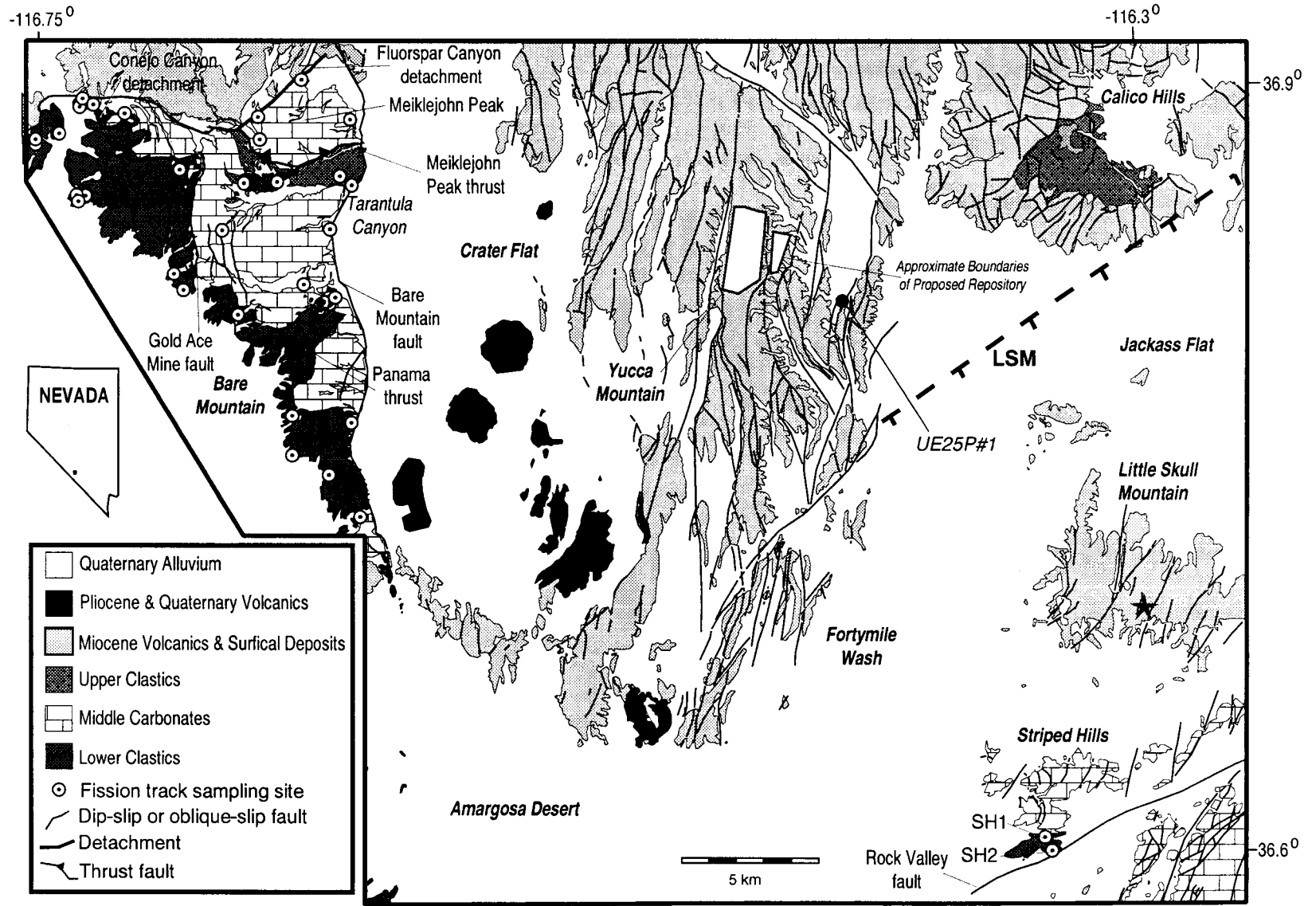
Fig. 14. West-east profile across northern Bare Mountain illustrating zircon and apatite fission track ages versus west-east position.

Fig. 15. Time line of tectonic events at Bare Mountain.

Fig. 16. (A) Slip tendency plot for Yucca Mountain area (after Morris et al., 1996) with poles to faults from Gold Ace Mine exposure in southwestern Bare Mountain (Fig. 7; after removal of northeastward plunge 042/37) and pole to M5.6 1992 Little Skull Mountain rupture plane overlain. (B) Slip tendency plot for Yucca Mountain overlaid with poles to nodal planes for the Little Skull Mountain earthquake and aftershocks illustrates close agreement between actual slipped planes and orientations of predicted high slip tendency (yellow to red colors). White triangles are poles to selected nodal planes and black triangles are poles to alternate planes as chosen by Harmsen (1994).

Table 1. Apatite fission track data from Bare Mountain and the Striped Hills, Nevada.

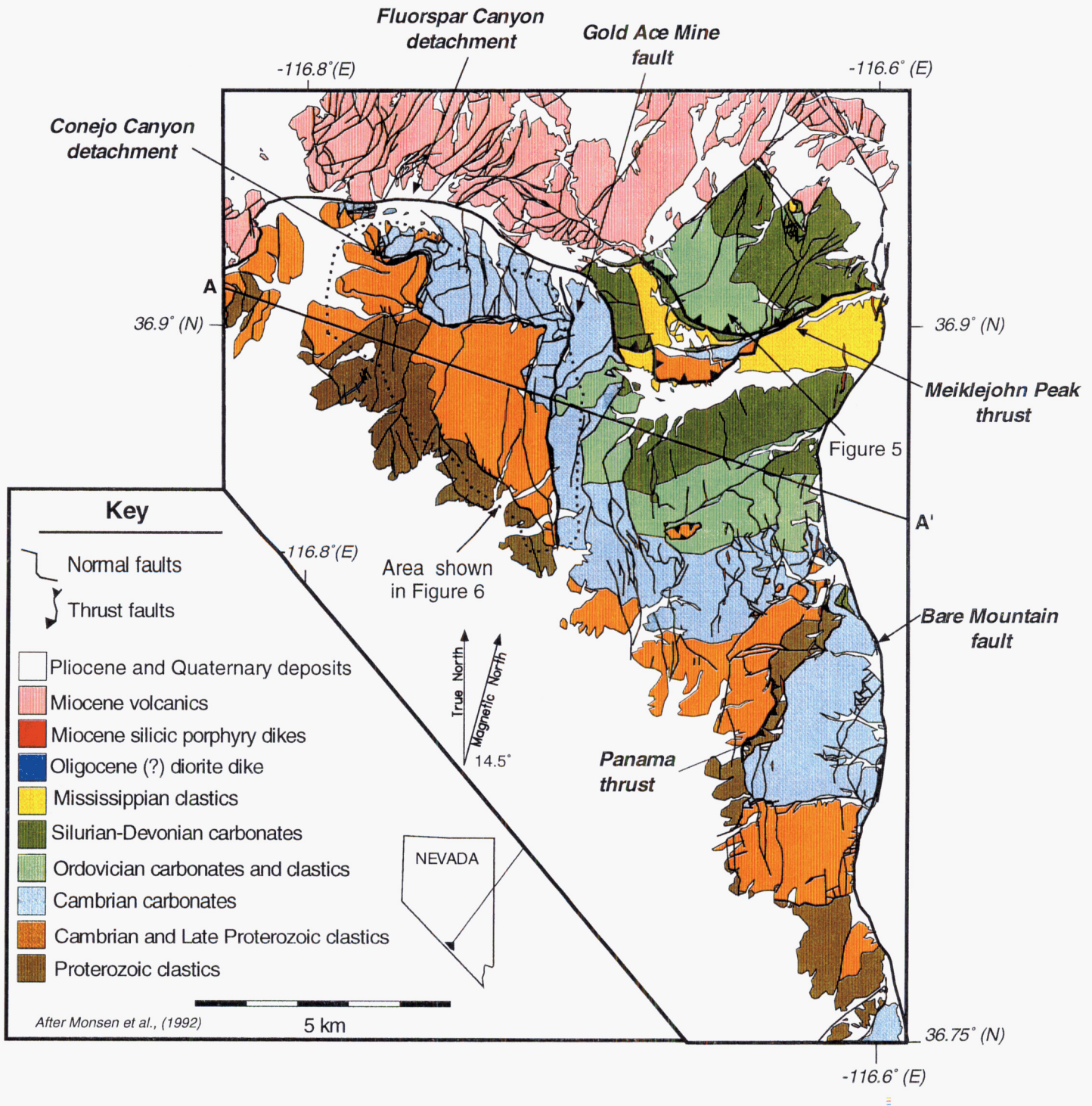
Table 2. Zircon fission track data from Bare Mountain, Nevada.



Ferrill et al., Geometric ...
Figure 1

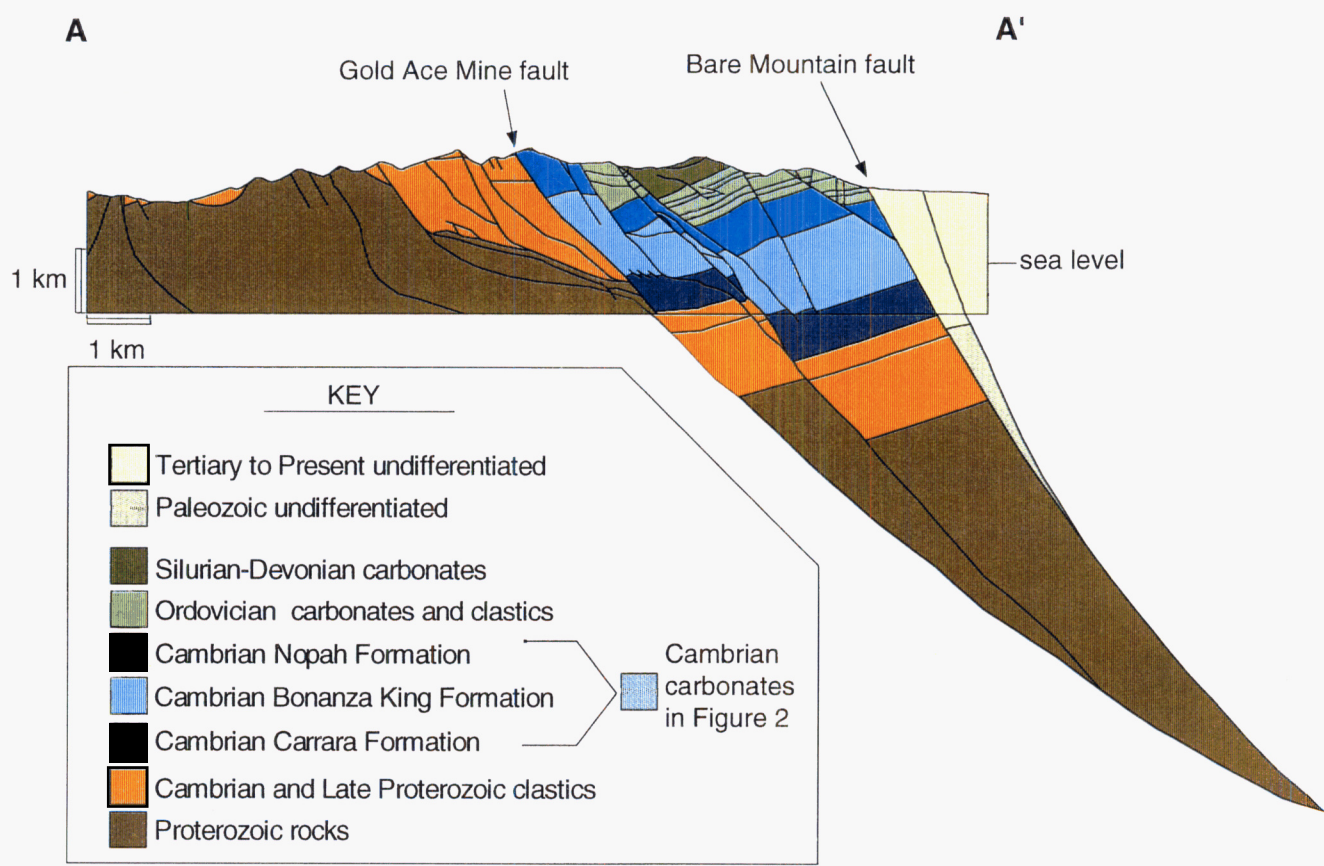
40/58

41/58



Ferrill et al.
Fig. 2

42/58



Ferrill et al.
Figure 3

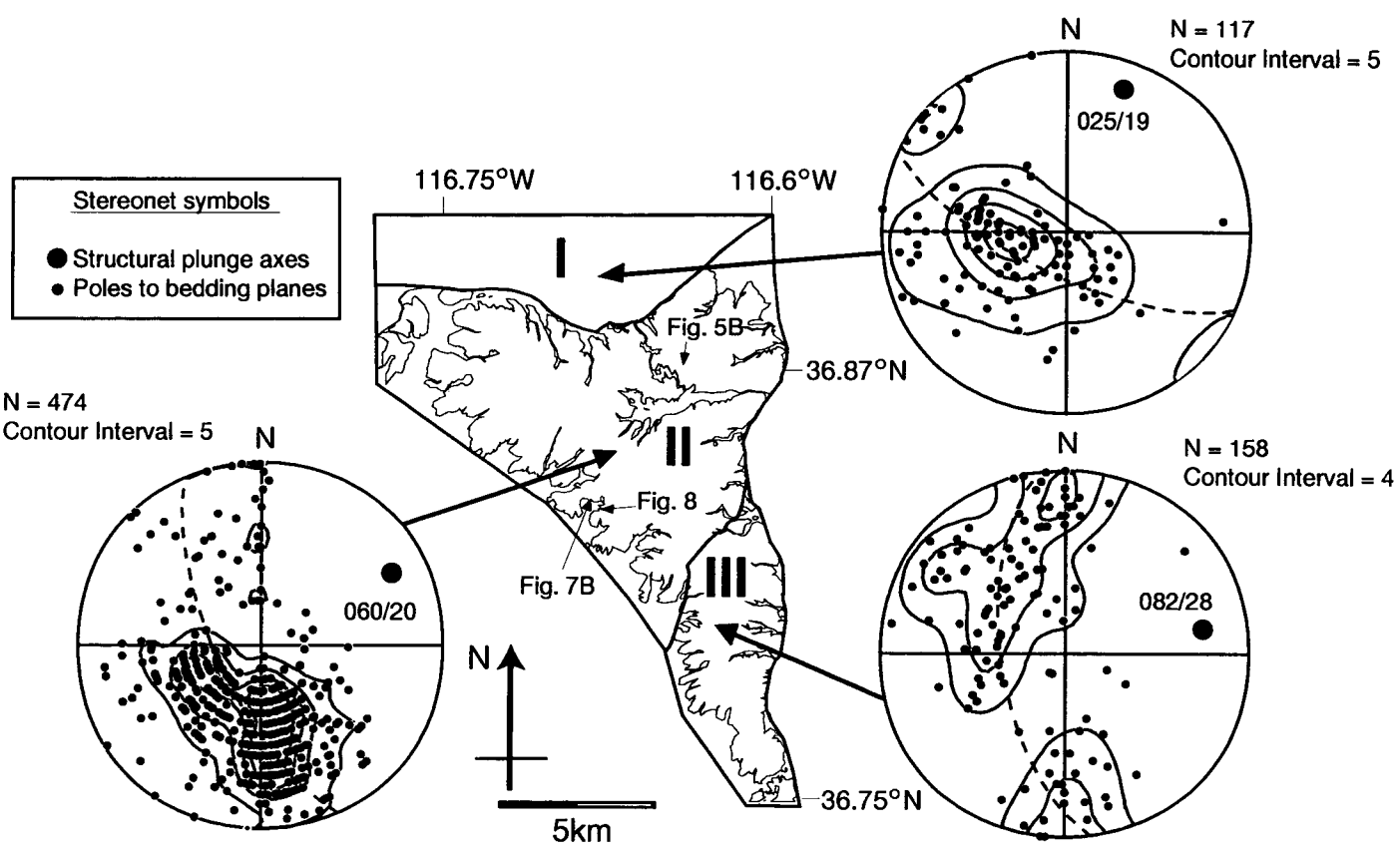
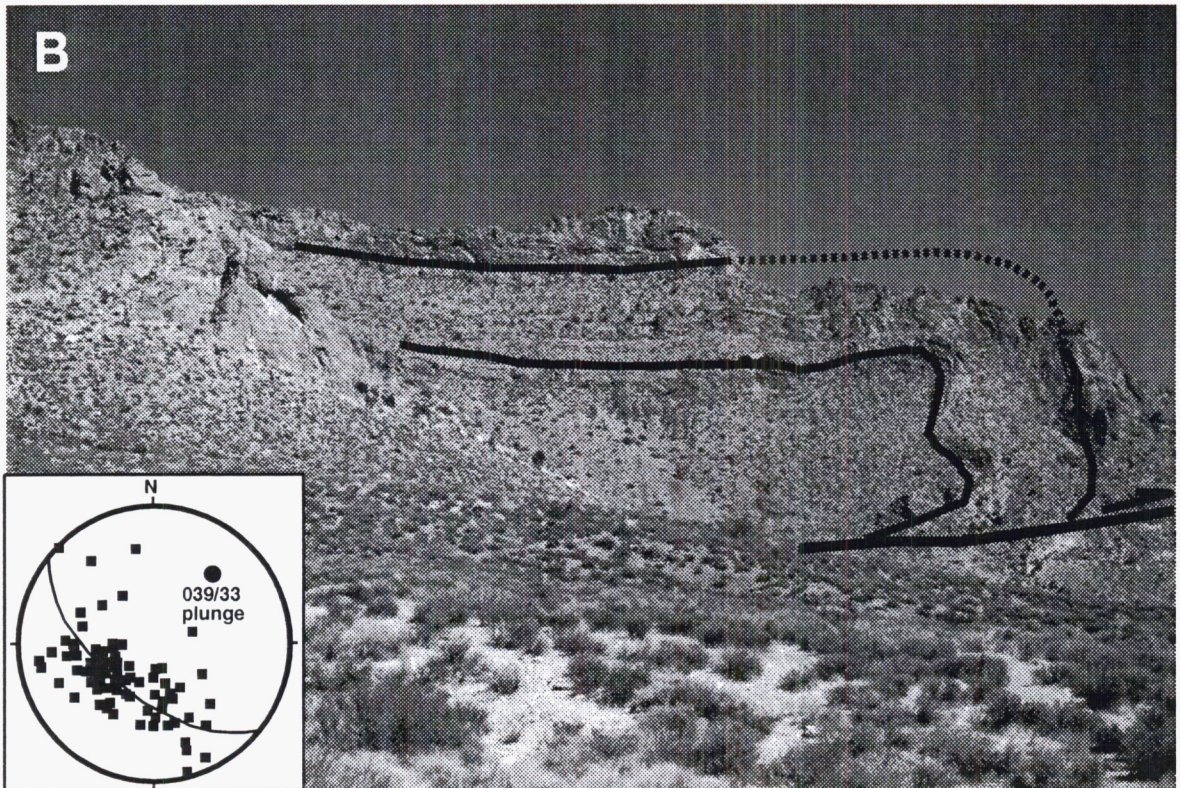
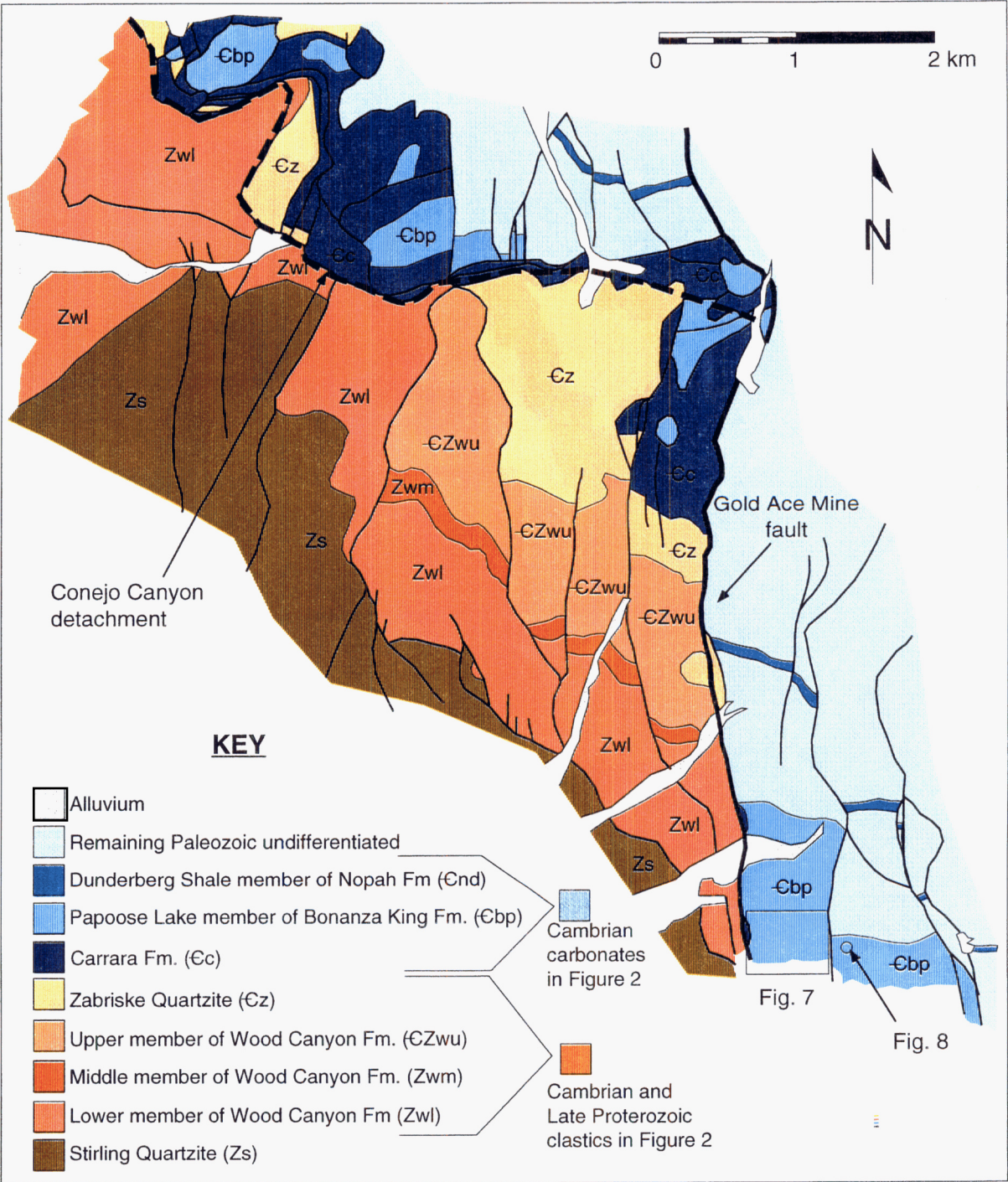


Figure 4
Ferrill et al.

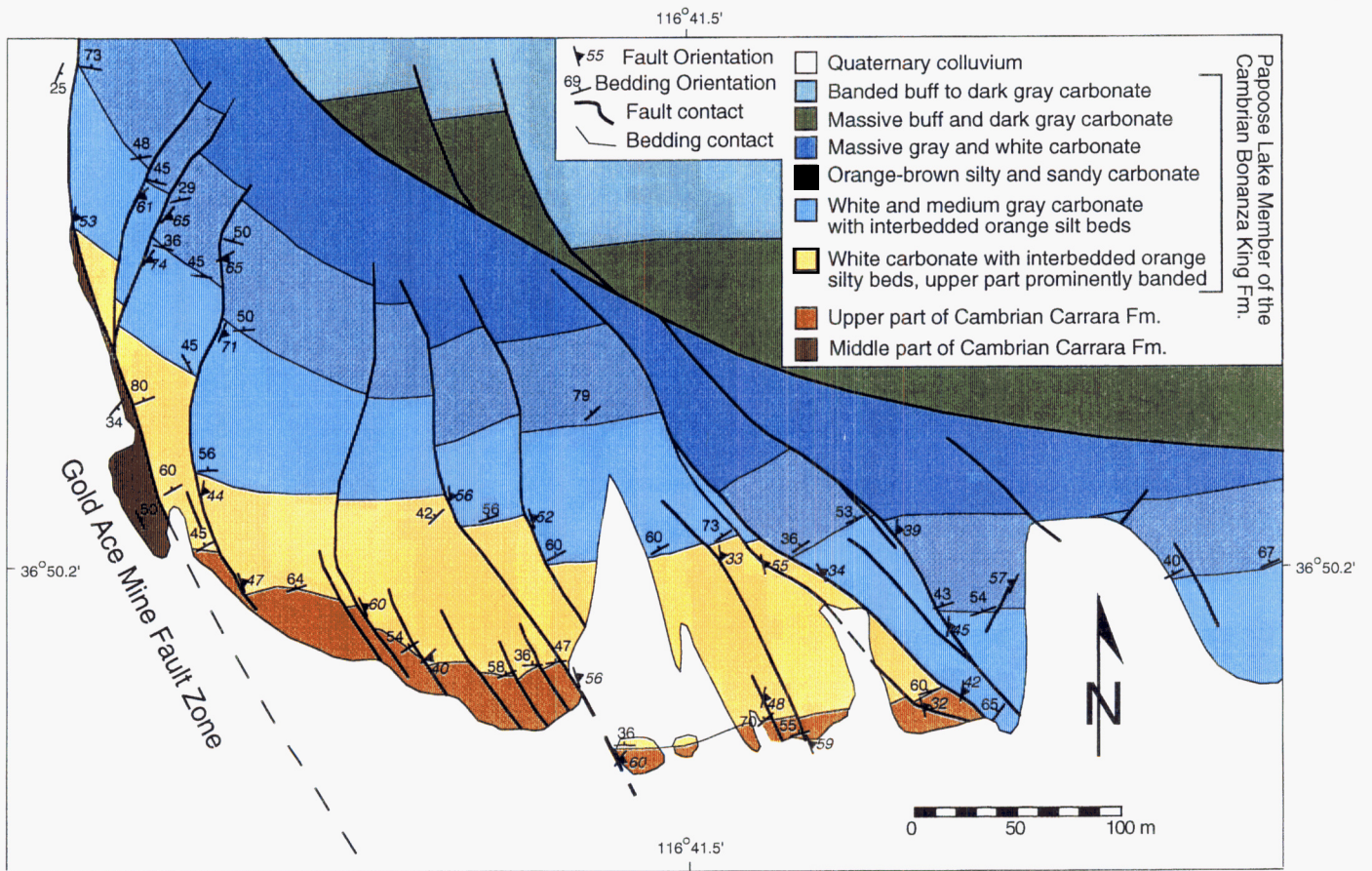


Ferrill et al.
Fig. 5



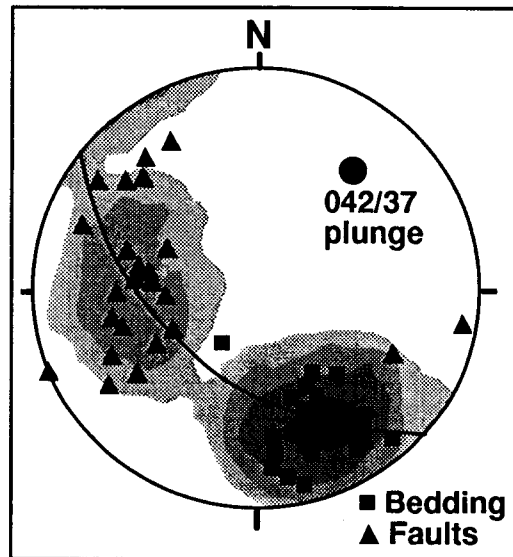
Ferrill et al., Geometric
Figure 6

46/58

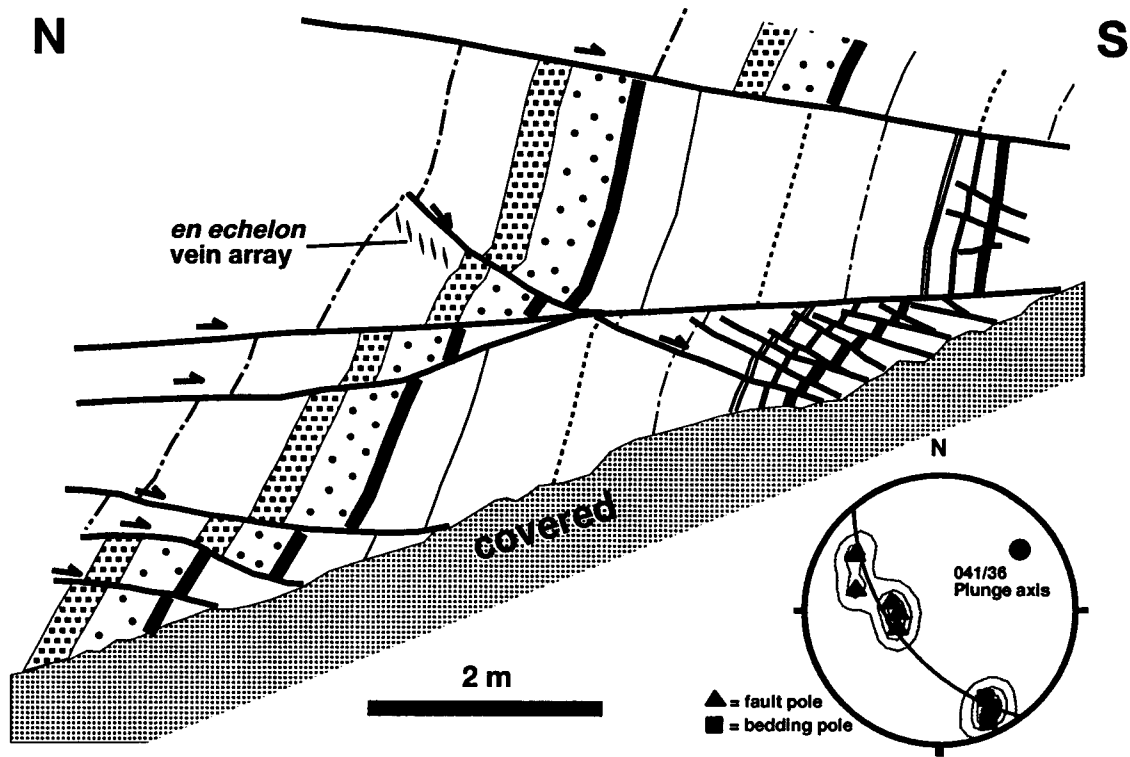


Ferrill et al.,
Figure 7a

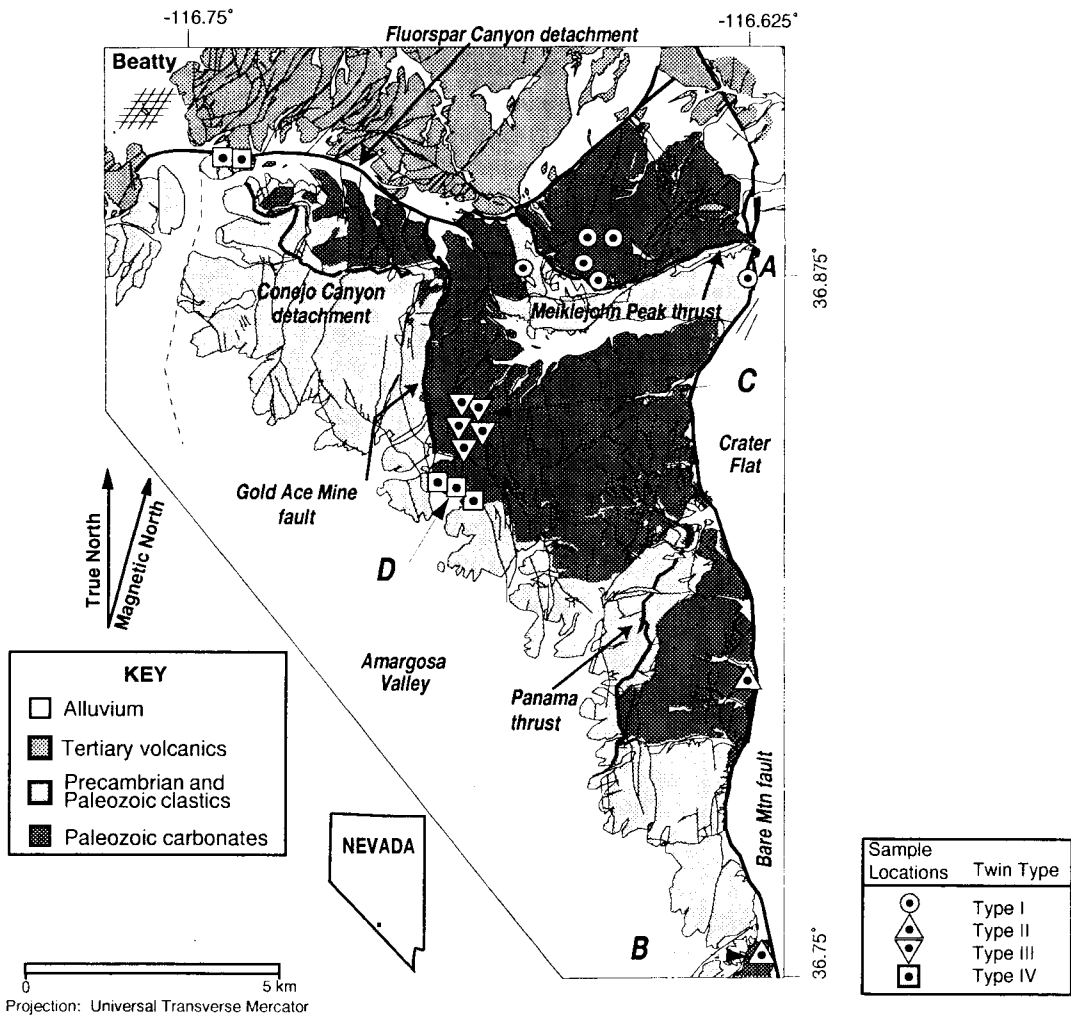
47/58



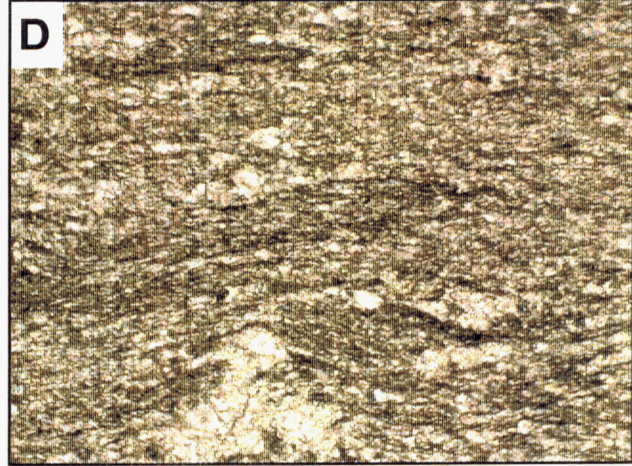
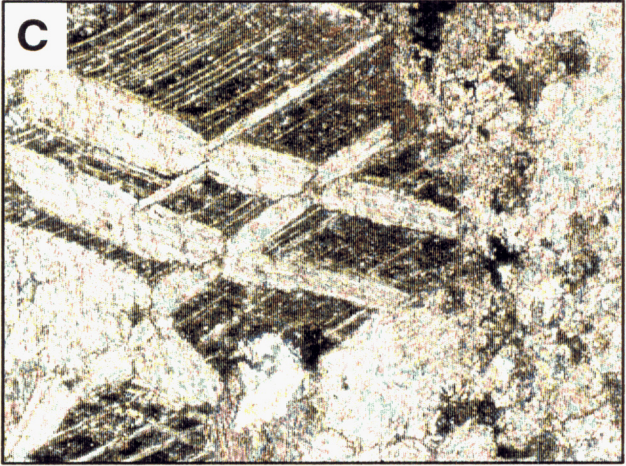
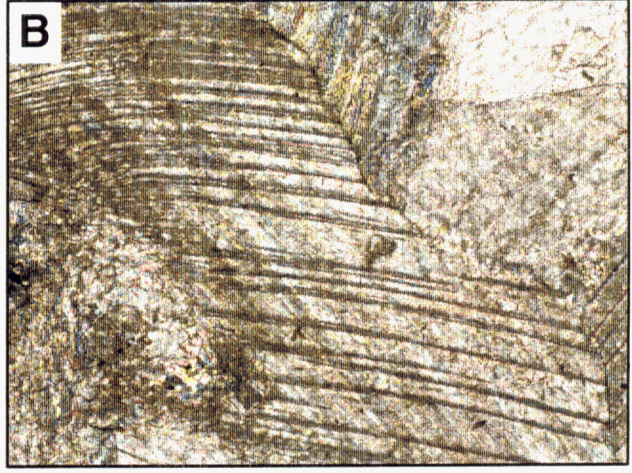
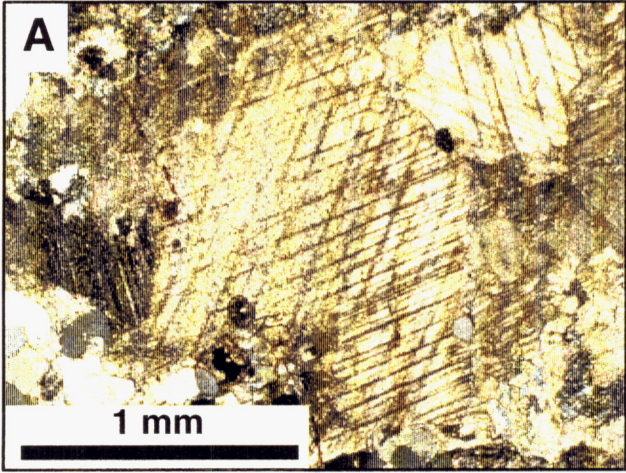
*Ferrill et al.
Figure 7b*



Ferrill et al.
Fig. 8

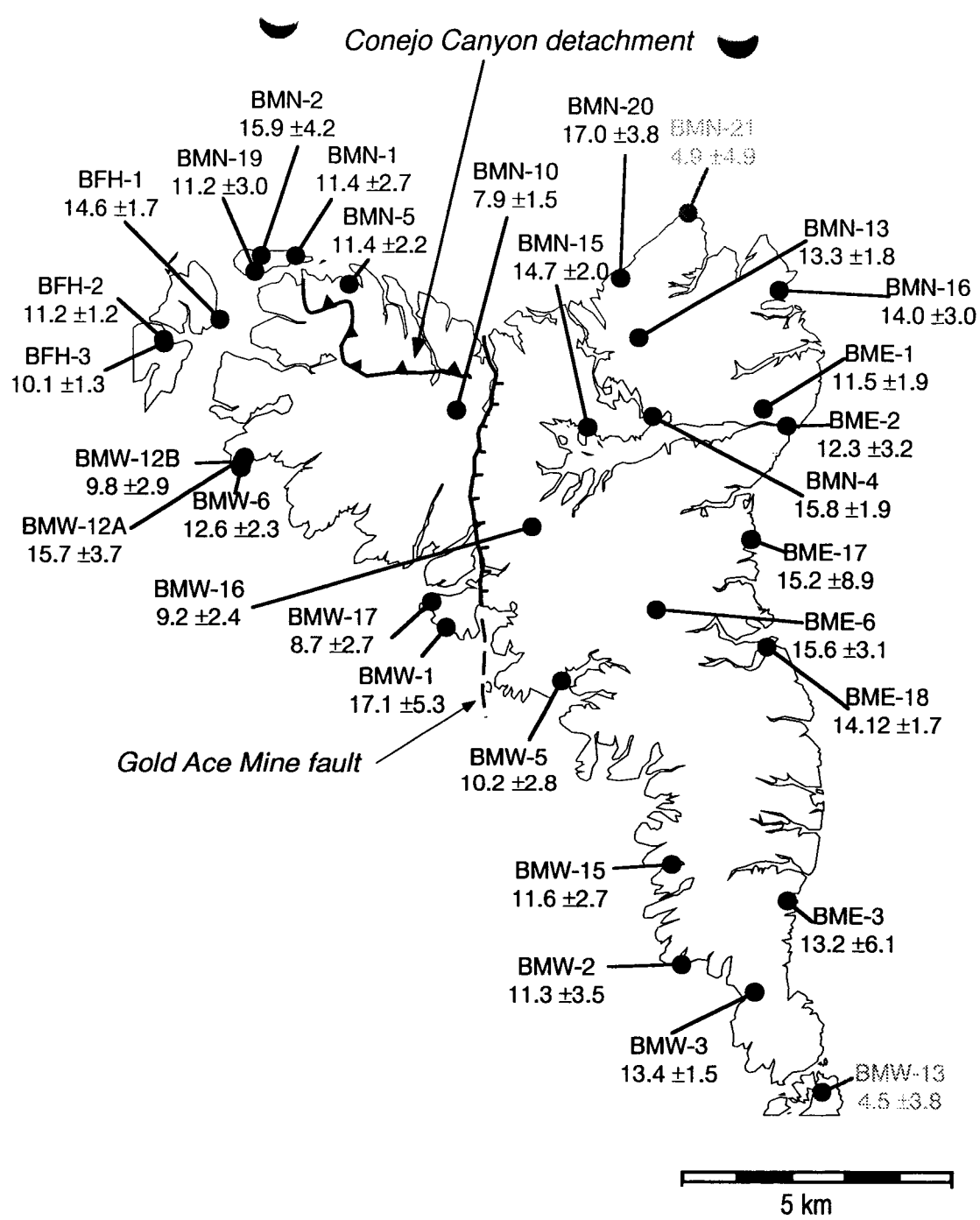


Ferrill et al.
Fig. 9



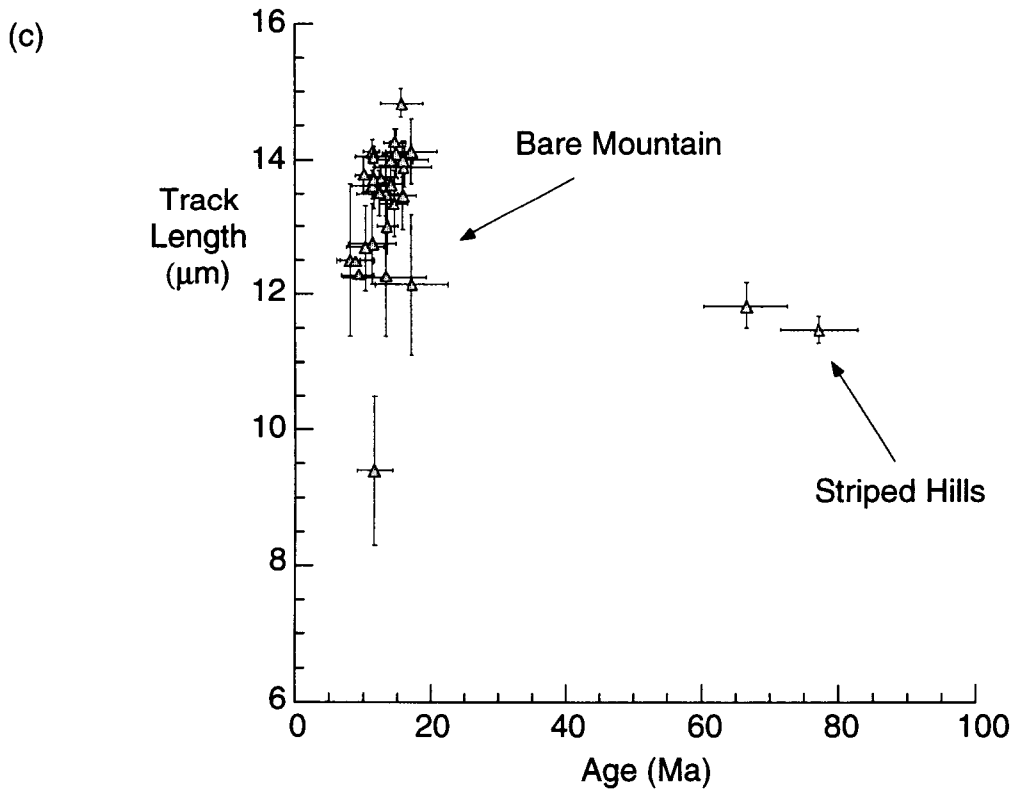
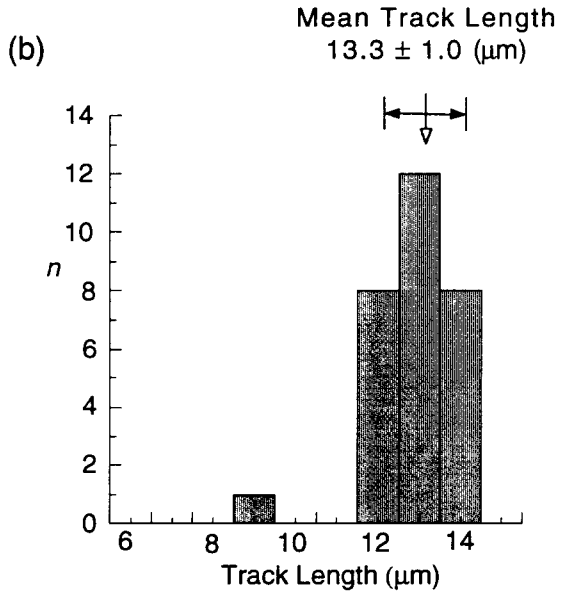
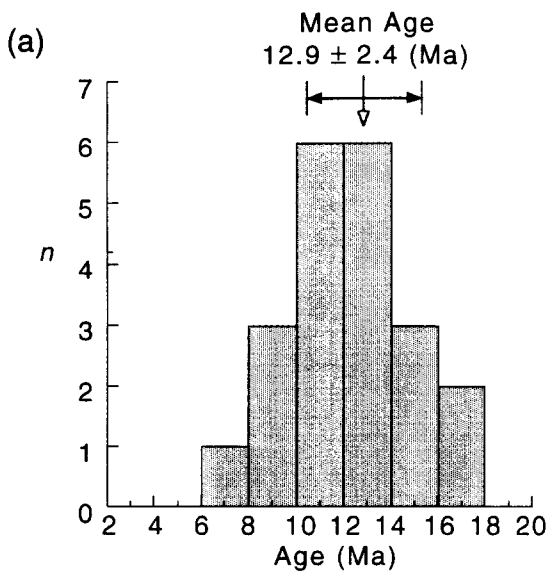
Ferrill et al.
Figure 10.

51/158

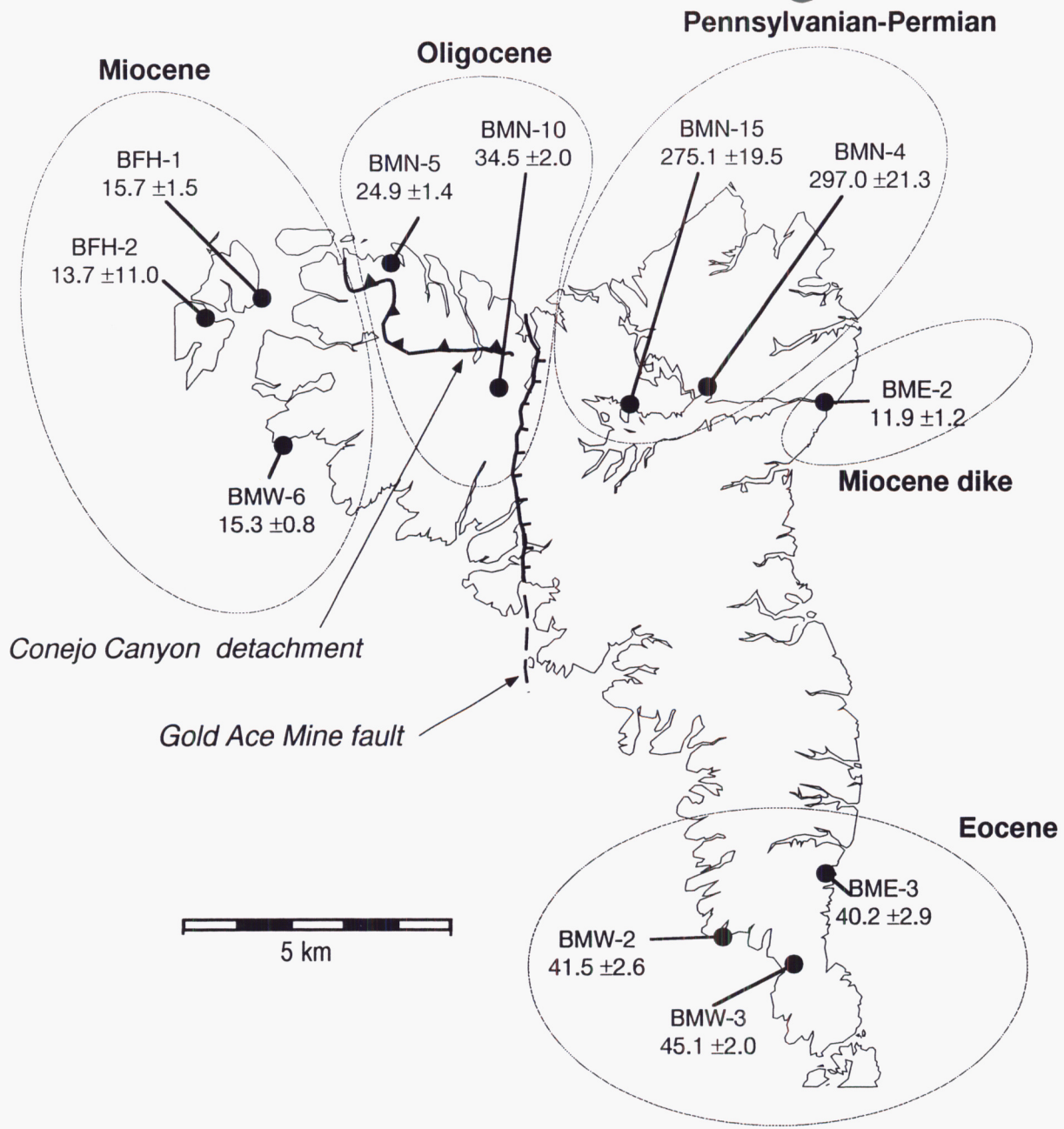


Ferrill et al.
Figure 11

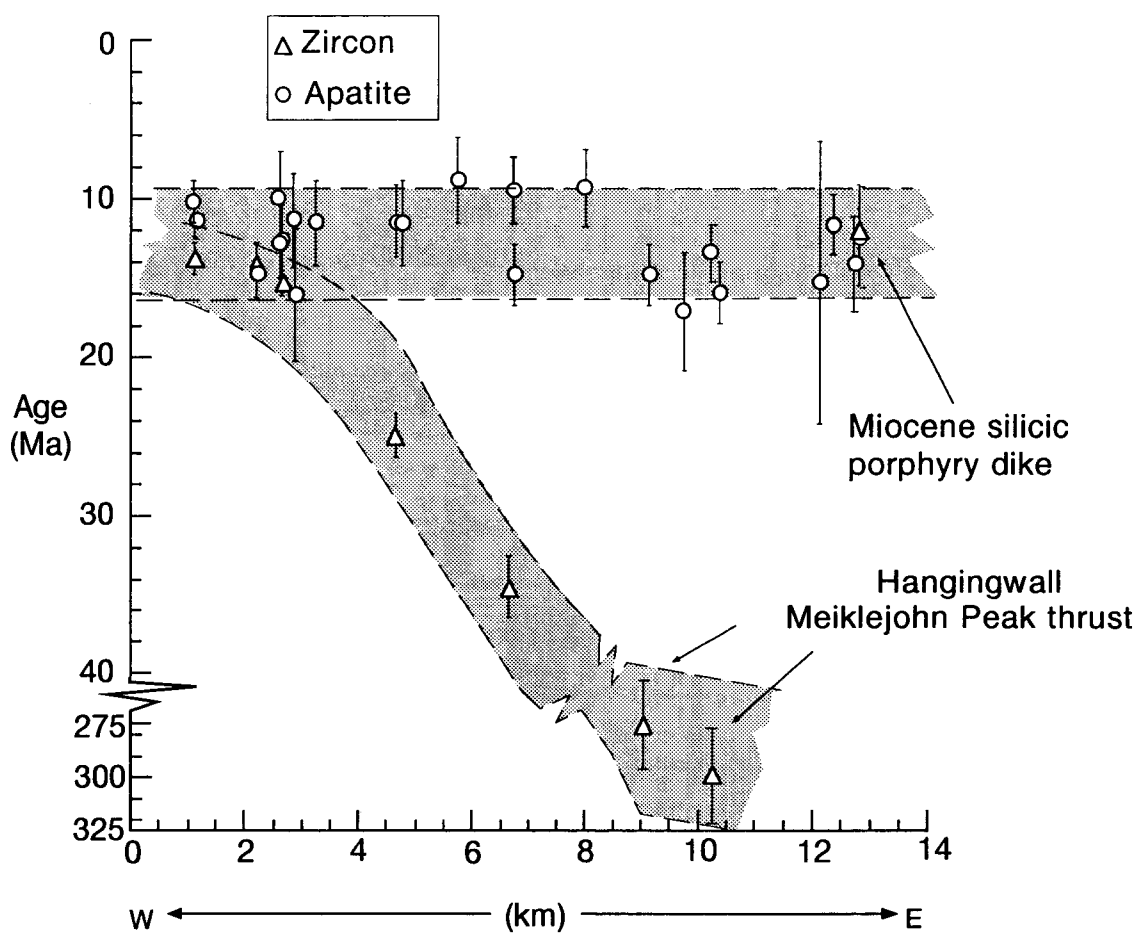
52/58



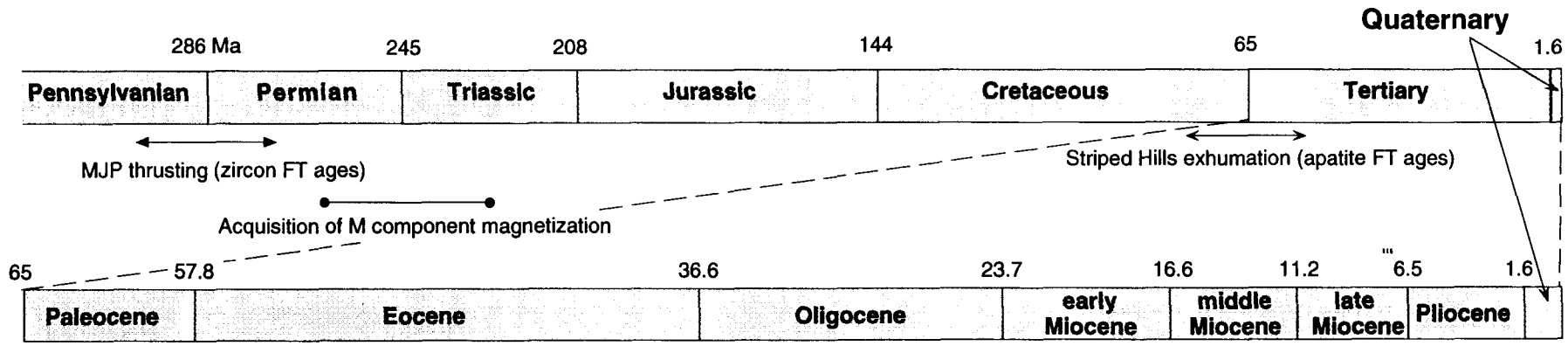
Ferrill et al., Geometric ...
Figure 12



Ferrill et al.
Figure 13



Ferrill et al., Geometric Figure 14



MJP thrusting (zircon FT ages) Striped Hills exhumation (apatite FT ages)

Acquisition of M component magnetization



? ← Tilting of Bare Mountain → Bare Mountain exhumation (apatite FT ages)
 ? ← Gold Ace Mine fault active → Fluorspar Canyon/Bullfrog Hills detachment system active
 ? ← Bare Mountain fault active →

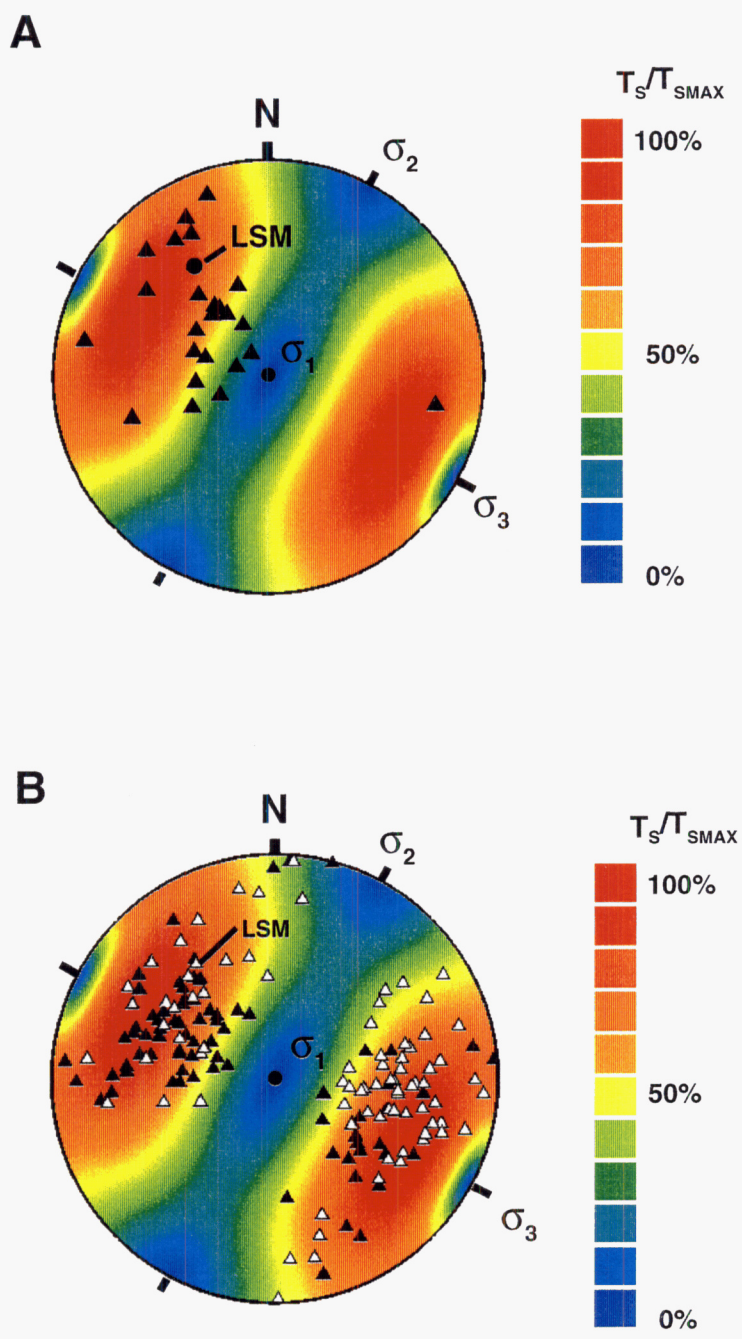
Intrusion of silicic porphyry dikes
 SWNVF silicic volcanism
 ? ← Basaltic magmatism →
 Epithermal & hydrothermal alterations
 Acquisition of H component magnetization

KEY

- ↔ Tectonism
- ↔ Faulting
- ↔ Igneous Activity
- Remagnetization or thermo-chemical effects

Ferrill et al., Geometric Figure 15

55/58



Ferrill et al.
Fig. 16

TABLE 1. APATITE FISSION TRACK RESULTS FROM BARE MOUNTAIN AND STRIPED HILLS, NEVADA.

Site	Rock Type	Elev.	r _s	N _s	r _i	N _i	r _d	N _d	N _G	Q	χ ²	Dpar	Pooled Age	Mean Age	N _T	Mean Length	σ	U
BF1	Czw (schist)	988	0.116	88	2.361	1792	5.238	4105	25	0.998	P	1.60	14.6 ± 1.7	14.7 ± 1.2	75	14.26 ± 0.19	1.61	23
BFH2	Czw (schist)	1073	0.127	96	3.390	2560	5.249	4105	25	0.210	P	1.58	11.2 ± 1.2	09.9 ± 1.5	101	14.12 ± 0.17	1.66	59
BFH3	Zs (quartzite D)	1091	0.095	66	2.810	1951	5.259	4105	22	0.129	P	1.66	10.1 ± 1.3	13.0 ± 2.4	51	13.79 ± 0.26	1.87	29
BMN1	Kg (granite)	1110	0.035	19	0.909	489	5.158	4105	25	0.729	P	1.61	01.4 ± 2.7	11.9 ± 3.2	51	14.05 ± 0.15	1.04	9
BMN2	Td (diorite)	1061	0.113	15	2.151	285	5.324	4105	18	0.945	P	1.65	15.9 ± 4.2	14.7 ± 5.1	33	13.91 ± 0.30	1.70	16
BMN4	Cz (quartzite)	1360	0.270	81	5.205	1559	5.335	4105	25	0.035	F	1.79	15.8 ± 1.9	20.2 ± 4.4	30	13.47 ± 0.51	2.75	57
BMN5	Cz (quartzite)	1232	0.049	28	1.311	749	5.345	4105	25	0.788	P	1.49	11.4 ± 2.2	13.4 ± 4.0	14	13.53 ± 0.51	1.84	15
BMN10	Cz (quartzite)	1677	0.219	31	8.421	1191	5.356	4105	13	0.177	P	1.65	07.9 ± 1.5	07.5 ± 2.9	14	12.51 ± 1.14	4.10	72
BMN13	Oe (quartzite)	1787	0.139	62	3.037	1351	5.086	4236	22	0.575	P	1.69	13.3 ± 1.8	13.6 ± 3.3	12	13.50 ± 0.59	1.94	34
BMN15	Cz (quartzite)	1610	0.279	58	5.471	1138	5.074	4236	15	0.788	P	1.73	14.7 ± 2.0	15.8 ± 2.7	18	14.09 ± 0.35	1.46	56
BMN16	Tl (latite)	1133	0.050	19	0.925	353	4.578	4116	24	0.706	P	1.70	14.0 ± 3.3	10.7 ± 3.0	47	13.99 ± 0.28	1.88	10
BMN19	Cz (quartzite)	1055	0.059	15	1.523	384	5.057	4236	23	0.207	P	1.61	11.2 ± 3.0	07.8 ± 3.4	83	13.63 ± 0.21	1.89	16
BMN20	Oe (quartzite)	1445	0.331	21	5.556	352	5.003	4236	9	0.774	P	2.16	17.0 ± 3.8	12.8 ± 5.2	12	14.13 ± 0.48	1.73	46
BMN21	Oe (quartzite)	1330	0.104	1	6.042	58	4.995	4236	1	n.a.	n.a.	1.55	04.9 ± 4.9	4.9	3	14.17 ± 0.75	1.06	56
BME1	Mde (congl)	1317	0.136	38	3.528	989	5.270	4105	25	0.143	P	1.61	11.5 ± 1.9	12.9 ± 4.5	12	13.72 ± 0.44	1.46	32
BME2	Tl (latite)	1226	0.035	15	0.857	368	5.287	4105	24	0.462	P	1.76	12.3 ± 3.2	11.6 ± 3.7	51	13.51 ± 0.35	2.51	8
BME3	Czw (schist)	1024	0.039	5	0.891	114	5.308	4105	9	0.900	P	1.50	13.2 ± 6.1	07.4 ± 6.0	11	12.26 ± 0.88	2.77	8
BME6	Tl (latite)	1660	0.038	27	0.641	451	4.576	4116	23	0.766	P	2.37	15.6 ± 3.1	16.0 ± 3.0	54	14.83 ± 0.21	1.50	7
BME17	Oe (quartzite)	1207	0.143	12	2.684	225	5.024	4236	11	0.594	P	1.57	15.2 ± 4.5	15.4 ± 8.9	0	n.a.	n.a.	29
BME18	Zs (quartzite E)	1189	0.250	79	5.032	1591	5.011	4236	24	0.930	P	1.67	14.1 ± 1.7	15.7 ± 1.8	30	13.64 ± 0.30	1.61	57
BMW1	Zs (schist C)	1128	0.026	11	0.440	189	5.173	4105	23	0.321	P	1.50	17.1 ± 5.3	19.0 ± 6.8	8	12.14 ± 1.04	2.76	5
BMW2	Zs (quartzite D)	976	0.027	11	0.707	286	5.190	4105	20	0.535	P	1.60	11.3 ± 3.5	16.1 ± 7.4	26	12.75 ± 0.60	3.02	11
BMW3	Zs (quartzite D)	997	0.161	92	3.563	2032	5.206	4105	24	0.575	P	1.57	13.4 ± 1.5	20.3 ± 3.3	26	13.00 ± 0.40	2.00	48
BMW5	Cz (quartzite)	1220	0.057	14	1.643	406	5.212	4105	22	0.238	P	1.60	10.2 ± 2.8	12.3 ± 5.8	8	12.70 ± 0.64	1.69	14
BMW6	Zs (quartzite D)	1049	0.072	33	1.630	752	5.045	4236	25	0.956	P	1.88	12.6 ± 2.3	11.3 ± 2.1	104	13.74 ± 0.18	1.81	17
BMW12A	Zs (quartzite D)	1098	0.094	19	1.830	369	5.367	4105	20	0.899	P	1.66	15.7 ± 3.7	18.1 ± 3.7	48	14.01 ± 0.26	1.76	17
BMW12B	Td (diorite)	1098	0.084	12	2.463	350	5.036	4236	14	0.575	P	1.56	09.8 ± 2.9	10.9 ± 4.0	0	n.a.	n.a.	22
BMW13	Zs (quartzite A)	939	0.013	2	0.800	125	4.987	4236	8	0.645	P	1.58	04.5 ± 3.2	04.3 ± 3.8	12	12.30 ± 0.67	2.24	8
BMW15	Zs (quartzite A)	1103	0.104	19	2.530	463	4.970	4236	18	0.840	P	1.75	11.6 ± 2.7	11.4 ± 2.8	2	0.49 ± 1.10	1.10	30
BMW16	Oe (quartzite)	1785	0.938	15	28.750	460	4.962	4236	2	0.343	P	1.68	09.2 ± 2.4	16.2 ± 10.4	1	12.29	n.a.	213
BMW17	Zs (schist C)	1170	0.110	11	3.576	357	4.953	4236	12	0.829	P	1.54	08.7 ± 2.7	05.7 ± 2.8	1	12.49	n.a.	32
SH1	Cz (quartzite)	1024	0.588	164	2.476	691	4.945	4236	14	0.038	F	1.99	66.4 ± 6.1	65.9 ± 9.8	43	11.83 ± 0.34	2.19	32
SH2	CZw (schist)	1012	0.768	290	2.781	1050	4.937	4236	25	0.320	P	1.97	77.1 ± 5.6	87.9 ± 8.3	148	11.47 ± 0.20	2.37	32

Notes: All errors are reported at 1σ; zeta calibration factor of 113.8 ± 2.9 (e.g. Hurford and Green, 1983) relative to CN-1 dosimeter glass (39 ppm natural uranium) determined using Durango and Fish Canyon Tuff apatite standards irradiated with these samples; mean spontaneous track lengths for Durango and Fish Canyon Tuff apatite standards are 14.47 ± 0.06 μm and 15.35 ± 0.06 μm respectively. Rock types are defined in Monsen et al., (1992). Elev is the elevation of the sampling site in m. r_s, r_i, and r_d, are spontaneous, induced, and dosimeter fission tracks, respectively, given in units of in 10⁶ tracks per cm². N_s, N_i, and N_d are the number of spontaneous, induced, and dosimeter fission tracks, respectively. N_G is the number of apatite grains. Q is the probability that χ² value would be greater than reported for a population of apatite grains having a common history and common kinetic response to that history; χ² Test, P (pass) for Q ≥ 0.05, F (fail) for Q < 0.05. Dpar is the mean etch pit diameter parallel to the crystallographic c-axis for the grains measured (Dpar < 1.75 typical of near-end-member fluorapatite). Pooled Age is the fission track age based on sum total of spontaneous and induced tracks for all grains measured (reliable when χ² Test is P) given in Ma. Mean Age is the arithmetic mean of the individual grain ages (reliable when χ² Test is F) given in Ma. N_T is the number of track lengths measured. Mean length is average track length in μm. σ is one standard deviation about the mean of the track length measurements. U is the concentration of ²³⁵U in ppm.

5/7/58

TABLE 2. ZIRCON FISSION TRACK RESULTS FROM BARE MOUNTAIN, NEVADA.

Site	Rock Type	Elev.	r_s	N_s	r_i	N_i	r_d	N_d	N_G	Q	X^2	Age	U
BFH-1	Czw (schist)	988	2.09	155	4.45	330	0.20	1272	11	0.89	P	15.7 ± 1.5	231
BFH-2	Czw (schist)	1073	2.80	246	7.46	664	0.20	1272	11	0.01	F	13.7 ± 1.0	385
BMW-6	Zs (quartzite D)	1049	2.58	554	5.37	1155	0.19	1223	20	0.16	P	15.3 ± 0.8	278
BME-2	Tl (latite)	1226	2.45	135	6.84	376	0.20	1260	8	0.56	P	11.9 ± 1.2	327
BMN-5	Cz (quartzite)	1232	2.73	579	3.58	759	0.19	1248	16	0.99	P	24.9 ± 1.4	184
BMN-10	Cz (quartzite)	1677	4.49	628	4.20	588	0.19	1235	20	0.56	P	34.5 ± 2.0	215
BMW-2	Zs (quartzite D)	976	6.31	606	4.84	465	0.19	1223	13	0.37	P	41.5 ± 2.6	266
BMW-3	Zs (quartzite D)	997	5.10	1291	3.60	911	0.19	1217	17	0.24	P	45.1 ± 2.0	187
BME-3	Czw (schist)	1024	3.61	419	2.97	344	0.20	1260	16	0.60	P	40.2 ± 2.9	153
BMN-4	Cz (quartzite)	1360	18.36	1964	2.04	216	0.19	1248	20	0.34	P	297.0 ± 21.3	107
BMN-15	Cz (quartzite)	1610	16.50	2230	1.94	221	0.19	1235	20	0.28	P	275.1 ± 19.5	100

Notes: Table headings are the same as in Table 1. Ages determined using $\zeta = 335 \pm 20$ for dosimeter glass SRM 962a (e.g., Hurford and Green, 1983). The age for sample BFH-2, which failed the X^2 test, is the mean age instead of the pooled age.

58/58